MOLECULAR TRANSPORT INTO THE OUTER MEMBRANE OF GRAM-NEGATIVE BACTERIA

A Dissertation
Presented to
The Academic Faculty

By

Karl P. Lundquist

In Partial Fulfillment
of the Requirements for the Degree
Doctor of Philosophy in the
School of Physics

Georgia Institute of Technology

May 2019

MOLECULAR TRANSPORT INTO THE OUTER MEMBRANE OF GRAM-NEGATIVE BACTERIA

Approved by:

Dr. James C. Gumbart, Advisor
School of Physics
Georgia Institute of Technology

Dr. Simon Sponberg
School of Physics
Georgia Institute of Technology

Dr. Ingeborg Schmidt-Krey
School of Biological Sciences
Georgia Institute of Technology

Dr. Nicholas Noinaj
Department of Biological Sciences
Purdue University

Dr. Bridgette Barry
School of Chemistry and Biochemistry
Georgia Institute of Technology

Date Approved: November 28, 2018

It’s funny how, day by day, nothing changes... but when you look back, everything is different.

Calvin and Hobbes

I dedicate this thesis to my parents, Phil and Priscilla Lundquist for all their love and support and very patiently waiting for me to start supporting them.

ACKNOWLEDGEMENTS

It is no exaggeration to say that getting this degree has been the most challenging experience of my life, and oftentimes in ways I could have never expected. There is no way I would have made it through this process without all the wonderful people who have been in my life providing me with encouragement and a voice of reason. Thanks to my parents and my sister, Kolina Mako for instilling a love for learning from a very young age. Thank you JC for your patience, intellectual and financial support, always practical guidance, and believing in me even when I didn't believe in myself. Thanks Anthony, Curtis, Sunny, and Anna for patiently answering all of my questions and listening to me complain. Thanks David, Zijian, and Katie for being the most hard-working grad students I could ask for to help me with the final push and for giving me the confidence that my unfinished projects will be left in good hands. Thanks Isabel Fernandez for being there for helping me understand all the biology concepts I never got the opportunity to learn in classes. Thanks to all of my friends at Zouk Atlanta for providing endless positively and encouragement, and a fun, lively space for me to cultivate my favorite hobby and maintain a bit of my soul and sanity. Thanks to all my wonderful friends who have been there for me throughout the process. Travis, Keshav, Dogukan, Gorman, Evan, and so many more. Finally I would like to thank my committee members who have all taken time out of their busy schedules to provide me with guidance and invaluable feedback on my research.

TABLE OF CONTENTS

LIST OF TABLES

LIST OF FIGURES

SUMMARY

This thesis details novel insights gleaned from the application of molecular dynamics (MD) simulations to two protein systems, the β-barrel assembly machinery (BAM), and the lipopolysaccharide transport machinery (LPT) involved in the transport of vital molecular components of the outer membrane of Gram-negative bacteria. Through the subsequent chapters we discuss the revelation of key insights into the function of these molecular machines. We reveal that the central member of the β-barrel assembly machinery requires a kinked C-terminal strand for proper function. We also describe differences in the extent of dynamics of the β-barrel assembly machinery dependent on the conformational state and presence of a key protein member. Finally, we highlight important features of the lipopolysaccharide transport machinery governing the proper transport of the foremost protective element of Gram-negative bacteria.

CHAPTER 1
INTRODUCTION AND BACKGROUND

1.1 Bacteria

Bacteria are one of the oldest and most ubiquitous life forms on earth. The approximately 5×10^{30} bacteria on Earth form a biomass that exceeds that of all plants and animals combined [1]. In the human body, the number of bacterial cells outnumbers that of human cells [2]. Fortunately, our relationship with bacteria is nearly always mutually beneficial. Sometimes, however, certain bacteria will maximize their survival by developing traits called virulence factors that can cause illness or death [3]. In cases of infection by virulent bacteria, we must rely on our immune system response and antibiotics to eliminate the bacteria. In certain cases, these same bacteria can develop a resistance to the antibiotics used to treat them in what is becoming an increasingly critical global health crisis. The CDC estimates that in the U.S. alone, over 23,000 people die each year due to antibiotic resistant infections, and many more die from other conditions complicated by an antibiotic resistant infection [4]. In light of this crisis, the development of novel antibiotics is more urgent than ever. This thesis presents unique insights gleaned from molecular dynamics (MD) simulations into the function of two vital protein systems. Each of these protein systems is surface exposed and involved in the transport of critical molecular components to the cell surface. As such, these systems are indispensable for the function of Gram-negative bacteria, and attractive targets for the development of future antibiotics [5, 6, 7, 8, 9].

1.2 Types of bacteria

Nearly all bacteria can be divided into two main groups based on their retention of crystal violet dye in what is called a Gram-stain protocol [10, 11]. Gram-positive bacteria have a single membrane surrounded by a surface-exposed peptidoglycan cell wall which is able to absorb and retain the crystal violet dye. Gram-negative bacteria possess an additional, asymmetric outer membrane (OM) surrounding a cell wall and a symmetric inner membrane (IM), such that the crystal violet dye is not absorbed [12, 13]. There is significant interest in understanding processes at the outer membrane to enable the development of antibiotics that can disrupt these processes without having to first cross the robust two-membrane barrier of Gram-negative bacteria. The most important processes occurring at the surface-exposed outer membrane are the insertion and assembly of outer-membrane proteins (OMPs) by the β-barrel assembly machine (BAM), and the insertion of lipopolysaccharides (LPS) by the LPS transport (LPT) machinery.

1.3 Components of Gram-negative bacteria

Gram-negative bacteria are distinguished from other cell types primarily based on the composition of their cell envelope. In addition to its unique architecture, the cell envelope also contains two unique classes of molecular components, β-barrel outer membrane proteins (OMPs), and lipopolysaccharides (LPS) [12, 13]. In this thesis we discuss molecular insights into the assembly of these components.

1.3.1 Proteins

Proteins are the molecular machines responsible for accomplishing the tasks which bring a cell to life. Nearly all antibiotics work by partially or fully disabling one of the protein machines in the target cell. Knowing how these proteins work can help enable the process of designing drugs or antibiotics to inhibit the function of these proteins. A protein is a

chain of amino acids connected by covalent peptide bonds. Each of these amino acids is composed of between ten and 27 atoms and has a common set of backbone atoms as well as a unique sidechain which gives each amino acid its special property. Some of the unique properties of amino acids are their size, charge, affinity to water, and their flexibility. This unique sequence of amino acids with its organization of these features give a protein its ability to fold into its predetermined shape and accomplish its designated function.

1.3.2 Outer membrane proteins (OMPs)

One of the most common ways a protein can fold is into what it called a β-sheet. In a β-sheet the peptide chain creates hydrogen bonds with the backbone of its neighboring strand. If you take a β-sheet and wrap it around such that the first and last strands connect, it is called a β-barrel. Nearly all outer membrane proteins (OMPs) in Gram-negative bacteria have a β-barrel domain that crosses the outer membrane. After being synthesized inside the cell by the ribosome, they are handed off to the Sec machinery which sorts proteins and passes the unfolded OMPs off to chaperones. These chaperones help to keep the OMPs from folding too early and help deliver them to the BAM complex for folding.

1.3.3 Lipopolysaccharides (LPS)

Lipopolysaccharides (LPS) provide the outer membrane (OM) of Gram-negative bacteria with a strong protective barrier. LPS molecules are similar to phospholipids in that they possess both hydrophobic and hydrophilic moieties and as such are able to form membranes, but they typically have a much more intricate composition. The hydrophobic domain is called lipid A and consists of around six acyl lipid tails. Attached to the lipid A is the core-oligosaccharide (OS), which is composed of several sugars and phosphate groups which form a tightly packed layer by coordinating divalent cations such as Mg^{2+} and Ca^{2+}. Finally a long sugar chain called the O-antigen protrudes from the core-OS. The composition of each of these domains can vary wildly as each species and strain finds its own

unique solution to best utilizing a protective LPS outer layer.

1.4 The assembly of OMPs

Outer membrane proteins follow an intricate path as they proceed to their final folded destination in the outer membrane. Several protein machines have been implicated in assisting in their assembly including periplasmic chaperones and other outer membrane proteins. The most important, and well-conserved of these machines is the β-barrel assembly machinery [14].

1.4.1 β-barrel assembly machinery (BAM)

The β-barrel assembly machinery (BAM) is the primary machinery responsible for folding β-barrels into the outer membrane. In E. coli it is composed of five proteins, BamA through BamE which each play a role in efficient assembly of OMPs, but only BamA and BamD are essential for cell viability [15, 16]. Crystal structures have been solved for each of these proteins both individually and more recently in a full complex [17, 18, 19].

1.4.2 BamA, the centerpiece

BamA is the central member of the complex that is thought to play the largest role in catalyzing the assembly of OMPs. The best ideas for how OMPs are assembled are supported by the unique features of the BamA β-barrel domain, and more specifically, the region where the first (β1) and last (β16) strands connect, known as the barrel seam. The first of these features is known as the C-terminal kink. For the structures exhibiting this C-terminal kink, the β1 and β16 strands interact weakly with only two hydrogen bonds formed between them, and the β16 C-terminal strand bends into the interior of the BamA β-barrel at a flexible glycine (G807) [20]. The second of these features is that, due in part to the weak connection between the first and last strands, previous simulations showed spontaneous separation to occur at the BamA β-barrel seam. In order to verify that this separation

event is important for function, the two strands were locked together with a disulphide cysteine mutation at several points along the seam. These mutations were shown to be lethal to bacteria, indicating that gate opening is likely important for BamA function [21]. Any membrane protein needs to have a band of externally facing hydrophobic residues so that it can interact favorably with the hydrophobic lipid tails of the membrane and stably occupy its position in the membrane. The third feature of the BamA β-barrel is that this band of hydrophobic residues near the seam is considerably thinner than the membrane. As such, it causes a localized distortion and thinning of the membrane which is proposed to reduce the barrier for the integration of substrates [20]. Based on these features, several models have been proposed to explain how BamA assists in the assembly of OMPs.

1.4.3 Models for OMP integration

Assisted model

It has been well-established that OMPs are capable of self-assembling into lipid bilayers [22, 23, 24, 25, 26], but this assembly is significantly accelerated in the presence of BamA [27]. It has also been shown that OMPs assemble more quickly into thinner and disordered bilayer environments [27, 28]. The assisted, or passive model for OMP insertion asserts that the membrane thinning induced by BamA is the primary basis for accelerating the assembly of OMPs [15]. This model asserts that any role of BamA barrel opening plays a secondary role. This model is supported in part by the fact that for certain OMPs, the locking of the BamA β-barrel seam strands together does not effect its ability to accelerate folding [29].

Hybrid barrel model

A second prominent model for OMP assembly is the hybrid barrel, or the budding model. This model heavily utilizes the BamA barrel opening in that it proposes that the exposed backbone in the opening is used by substrates as a scaffold onto which the nascent OMP

will bind its own β-strands [30, 15, 31]. This would effectively cause the BamA β-barrel to grow into a larger hybrid barrel with some part, or the entirety of the substrate OMP being contained in its seam opening. After the assembly of all or some of the substrate strands, the nascent OMP would bud off from BamA to become a mature protein and carry out its designated function. A significant boon for the budding model arrived in a study published in early 2018 in which highly specific crosslinks consistent with the budding model were observed between Sam50, a mitochondrial homolog of BamA, and one of its substrates, VDAC [32].

1.5 The transport of LPS

LPS molecules have a complex architecture, and thus require a large number of protein systems to complete their assembly. At the cytosolic side of the inner membrane, the biosynthesis of lipid A is first performed by the Lpx protein family and core oligosaccharide is added by Waa proteins [33, 34, 35]. The partially assembled LPS is flipped across the inner membrane by the ABC transporter MsbA, the O-antigen chain is ligated, and finally transported across the periplasm by the LPS transport (Lpt) machinery.

1.5.1 The LPS transport (LPT) machinery

The periplasm-spanning Lpt machinery is responsible for the transport of LPS molecules across the periplasm, culminating in insertion by the outer-membrane proteins LptD and LptE. The Lpt machinery is a seven-protein complex consisting of LptA–G [36], all of which are essential [37]. At the inner membrane LptBFG is an ABC transporter which hydrolyzes ATP to transfer LPS from the inner membrane to LptC [38, 39]. LptC, -A, and -D each possess a β-jellyroll domain with a hydrophobic interior [40, 41]. These three proteins link together with hydrogen bonds along their β-strands to span the periplasmic space and shuttle LPS molecules using interactions between the hydrophobic groove and lipid A tails [42]. Finally, LptDE is thought to escort LPS to the outer membrane through

a separation between its first (β1) and last (β26) stands.

1.5.2 LptD/E

The first crystal structures for the LptD/E complex were released in 2014, revealing an unprecedented 26-strand β-barrel with an N-terminal "jelly roll" domain, and LptE as the plug domain for LptD [43, 41]. Unlike is the case for models of OMP assembly, the principal model for LPS transport, while in need of further refinement, is largely uncontested [44]. In this model, LPS, which exists in its fully assembled state at the outer leaflet of the inner membrane is transferred, using ATP, to LptC by the ABC transporter LptBFG [38, 39]. It is then bound by the periplasm spanning hydrophobic track created by LptC, -A, and -D which each possess a β-jellyroll domain with a hydrophobic interior [40, 41]. These three proteins link together with hydrogen bonds along their β-strands to span the periplasmic space and shuttle LPS molecules using interactions between the hydrophobic groove and lipid A tails [42]. The LPS molecules reach the inner surface of the outer membrane through a combination of diffusion and ATP hydrolysis energy where then LptD/E escorts LPS to the outer leaflet of the outer membrane by separating its first (β1) and last (β26) stands. However, unlike is the case for BamA, simulations of LptD failed to produce the spontaneous seam separation required for LPS passage, leading to uncertainty of the molecular signals prompting the insertion event.

1.6 Results outline

To gain further clarity of the mechanism of the transport and assembly of OMPs and LPS, we have performed a myriad of equilibrium MD simulations and PMF calculations of members of the BAM and LPT complex. We have analyzed the dynamics of the BamA β-barrel seam to determine that a kinked conformation of the C-terminal strand is required and that with this conformation lateral gate opening should occur spontaneously on a physiological timescale. In the second phase of this research project, we utilized simulations of BamA

in complex with its accessory proteins BamB, BamC, and BamE in order to investigate how the formation of the complex is able to modulate the dynamics of the BamA β-barrel seam. Finally, we determined several features along the path of the LPS insertion pathway by LptD/E which may be important for its insertion into the outer membrane.

1.6.1 C-terminal kink formation is required for lateral gating in BamA

In order to address the remaining questions surrounding OMP assembly by the BAM complex, we first focused on the factors influencing the flexibility of the BamA β-barrel seam. To do this we carried out a series of equilibrium molecular dynamics (MD) simulations of BamA and free-energy calculations of the energetic barrier to barrel opening under a number of different conditions [45, 46]. We then used these free energy measurements to determine a mean first passage time for the gate opening process. The results of these simulations are discussed in Chapter 2.

1.6.2 Lipoproteins act to stabilize the open state of the BAM complex

Using the newly released crystal structures of the full E. coli BAM complex to determine that the In the second phase of this research project, we utilized simulations of BamA in complex with its accessory proteins BamB, BamC, BamD, and BamE in order to investigate how these proteins modulate the dynamics of the complex and the BamA β-barrel seam. We have determined that the open state of the BAM complex is more dynamic, but the accessory proteins can stabilize this open state. The results of these simulations are included in Chapter 3.

1.6.3 Active features governing the LptD/E insertase

In order to elucidate the dynamics of LptDE governing the insertion of LPS substrates, we performed over 10 microseconds of equilibrium molecular dynamics simulations. From these trajectories we have performed a comparison of dynamics in DMPE and OM models,

which demonstrate bilayer-dependent differences in the fluctuation and secondary structure formation in the extracellular loops. We report significant results from our simulations related to conformational changes observed throughout the trajectories. An apparent flexibility results in a highly dynamic N-terminal domain. This may be required to maintain integrity of the periplasm-spanning complex amidst relative motion of the inner membrane and outer membrane anchored domains. We also observe significant motion of extracellular loop 4 which may be required to allow the passage of the LPS oligosaccharide region. Finally, we observe a switch-like association between two "so-called" luminal loops at the interface between the N-terminal domain and the putative LptD lateral gate. Dissociation of these loops may be the first step along the insertion pathway of LPS by LptDE via the LptD lateral gate. Several microseconds of equilibrium simulation and free energy calculation were performed on systems including LptD/E in symmetric and asymmetric bilayers [47]. These results are detailed in Chapter 4.

CHAPTER 2
C-TERMINAL KINK FORMATION IS REQUIRED FOR LATERAL GATING IN BAMA

2.1 Introduction

The folding and membrane insertion of β-barrel proteins is a process taking place in most cells, foremost among them, Gram-negative bacteria. These bacteria possess an outer membrane (OM) in addition to the more common cytoplasmic, inner membrane (IM). In contrast to the IM, the OM consists of a phospholipid inner leaflet, a lipopolysaccharide (LPS) outer leaflet, and is populated almost exclusively with β-barrel proteins [12, 48, 49]. Likely because of their bacterial origins, mitochondria and chloroplasts also possess two membranes with β-barrel proteins in their OMs [50].

2.1.1 Assembly of OMPs

Outer-membrane proteins (OMPs) regulate traffic into and out of Gram-negative bacteria including water, ions, nutrients, and, in pathogenic bacteria, virulence factors, and, are thus critically important for bacterial survival [13, 51, 52, 53]. Their surface exposure also makes them attractive antibiotic and vaccine targets, negating the need to breach one or both membranes. OMPs are synthesized in the cytoplasm, transported across the IM by the Sec translocon, and finally cross the periplasm with assistance from several chaperones [54, 55, 56, 57], before being assembled and inserted into the OM by the β-barrel assembly machinery (BAM) [58, 16, 59, 60, 61, 62, 14, 63]. The BAM complex is comprised of five proteins (BamA–BamE) whose structures have now been solved both individually and in complex [17, 19, 18, 64].

2.1.2 The centerpiece of the OMP assembly machine

The most essential component of the BAM complex is BamA, which has a C-terminal 16-stranded β-barrel domain as well as five N-terminal polypeptide transport-associated (POTRA) domains on the periplasmic side. Early structures and molecular dynamics (MD) simulations of BamA revealed three notable features [20]. First, in the *Neisseria gonorrhoeae* BamA structure, the interaction between the first (β1) and last (β16) strands of the BamA β-barrel is unexpectedly weak (Fig. 2.1). Second, equilibrium MD simulations indicated that a separation between the β-strands at the barrel seam could occur, producing a so-called "lateral gate" between the hydrophobic membrane environment and the aqueous β-barrel lumen. Recently, this "lateral gate" was also shown to exist in TamA, which is evolutionarily, closely related to BamA and assists in the assembly of some OMP substrates [46, 65, 66]. Third, a thin hydrophobic region in BamA near the lateral gate produced a destabilized membrane, which may decrease the barrier for OMP integration [67, 68, 28]. Together, these features have pinpointed the BamA barrel seam as the putative insertion point for nascent OMPs.

2.1.3 Models for OMP assembly

The BamA β1-β16 seam has become the centerpiece for several models for OMP assembly including the so-called "hybrid barrel model" [31, 15] and the "passive model" [29]. In the passive model, the principal role played by the seam is to prime the membrane for OMP insertion. In the hybrid barrel model, the seam functions as a gate for substrate passage and/or as a template onto which nascent β-barrels may assemble. However, little is known about the factors influencing the dynamics of the BamA seam. Now, using both long-time-scale equilibrium MD simulations as well as free-energy calculations, we have determined the likelihood of lateral gating at this seam under different conditions. Our simulations reveal, in particular, an important role played by the kinked conformation of β16 in modulating gating energetics observed in some, but not all, crystal structures of BamA [20, 69, 70].

This conformation significantly reduces the lateral-gate-opening energetic barrier and is the only persistent C-terminal conformation observed throughout over 11 μs of combined equilibrium simulations. Furthermore, we demonstrate that formation of the kink is important for maintaining BamA structure and function in mutagenesis experiments in which G807 of β16 is mutated to bulkier residues, rendering bacterial cells more susceptible to antibiotics.

2.2 Equilibrium simulations

To explore the equilibrium dynamics of the BamA β-barrel seam, we carried out simulations of two recent crystal structures from *N. gonorrhoeae* (NgBamA; PDB 4K3B with all POTRA domains removed) [20] and *E. coli* (EcBamA; PDBs 4N75 and 4C4V with only POTRA5 retained; see Methods) [69, 70]. EcBamA was simulated for over 4.2 μs in a simplified version of the outer membrane bilayer (OM) with lipopolysaccharide (LPS) in the outer leaflet and POPE in the inner leaflet; NgBamA was simulated for over 7 μs in total in three different membranes, namely POPE only, DLPC only, and OM (see Table 4.1 and Fig. A.1). DLPC has been used in a number of the experimental studies of OMP folding in membranes [71, 24, 55], while POPE is a common membrane used in simulation studies of OMPs [72, 73]. In these simulations, we observed several novel behaviors of the N- and C-terminal strands and the surrounding region, including C-terminal kink formation, lateral gate opening, and membrane thinning. Notably, these behaviors are not specific to the membrane used, validating in part the use of other membranes experimentally and computationally.

2.2.1 C-terminal kink formation

In the four available crystal structures of BamA alone [20, 69, 70], two present with a C-terminal kink, in which the C-terminal β-strand bends into the lumen, leaving only 2-3 hydrogen bonds at the N/C-terminal-strand interface instead of 6-8 in the "zipped" confor-

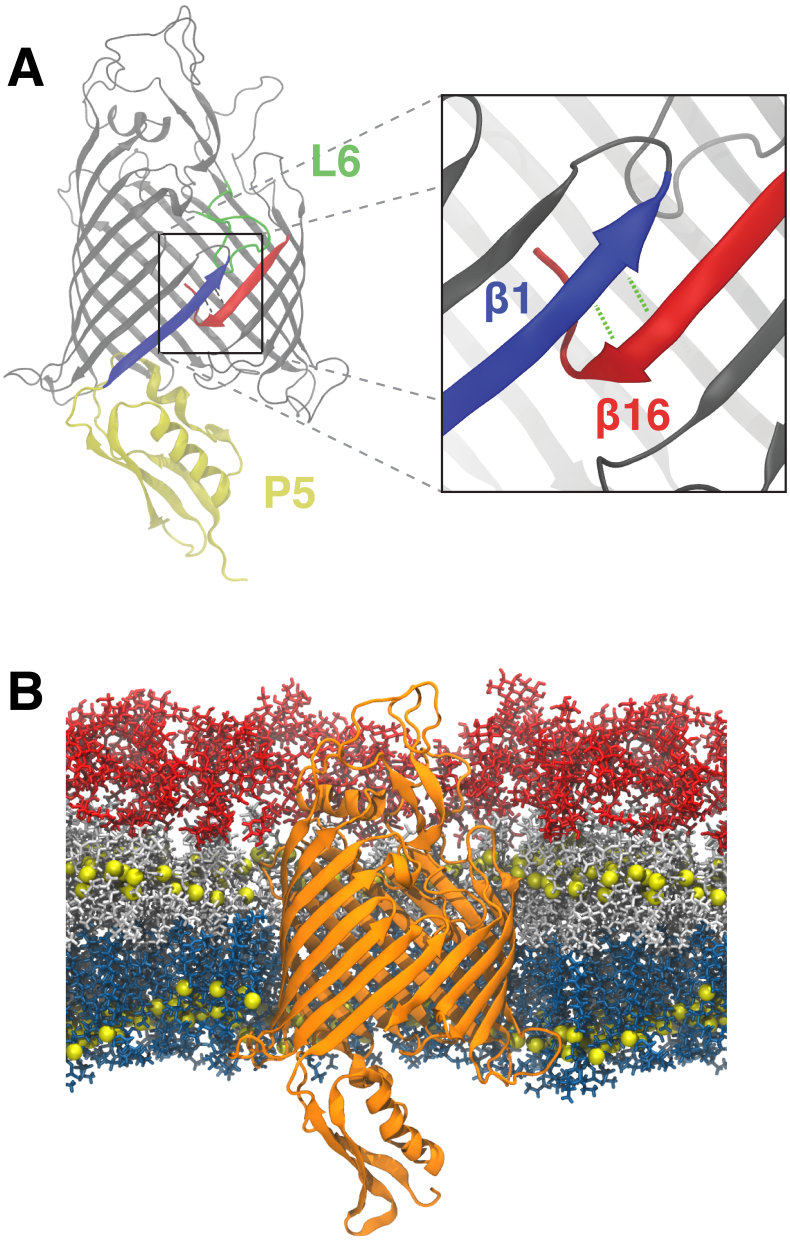

Figure 2.1: Features of BamA highlighted. (A) First (β1) and last (β16) β strands, which form the lateral gate, shown in blue and red, respectively. β16 is shown in the kinked conformation. β-barrel and P5 domain of BamA with β1 (blue), β16 (red), P5 (yellow), and L6 (green) domains highlighted. (B) EcBamA in OM system (NgBamA in OM is not shown) used for equilibrium simulations. Protein is shown as orange ribbons; C2 (and C4 for LPS) atoms which delineate the hydrophobic region, are shown as yellow spheres; phospholipids are shown as blue sticks; and lipid A and core oligosaccharide regions of LPS are shown in white and red, respectively.

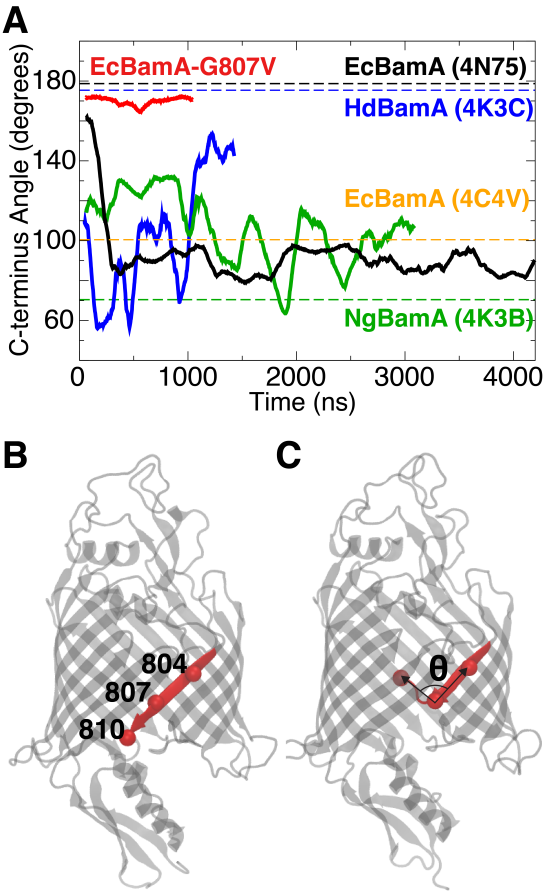

Figure 2.2: C-terminal kink formation in BamA. (A) Plot of the angle formed by the C_α of residues 804, 807, and 810 throughout the simulation (*E. coli* numbering). These residues are shown as red spheres in cartoon renderings of the (B) zipped and (C) kinked C-terminal strand conformations. For reference, the angles formed in crystal structures are shown as dotted lines, while simulation trajectories are solid lines. Trajectories shown are EcBamA-OM-310 (black), NgBamA-OM-340 (green), HdBamA (blue), and EcBamA-G807V (red). HdBamA trajectory data is from Noinaj et al. [20]. Average values for C-terminal kink angles were 92.6±16.7° for EcBamA, 103.6±35.7° for HdBamA, 106.0±20.8° for NgBamA, and 170±4.7° for G807V.

Table 2.1: A summary of equilibrium simulations performed for this study. Because PDB 4N75 lacks the fifth POTRA domain, P5 from PDB 4C4V was added to create the EcBamA system (see Appendix A.5.2).

Label	PDB	Species	Time (ns)	Membrane	Temp. (K)
EcBamA-OM-310	4N75, 4C4V	*E. coli*	4255	OM	310
NgBamA-OM-340	4K3B	*N. gonorr.*	3146	OM	340
NgBamA-POPE-310	4K3B	*N. gonorr.*	986	POPE	310
NgBamA-DLPC-310	4K3B	*N. gonorr.*	986	DLPC	310
NgBamA-DLPC-340	4K3B	*N. gonorr.*	2102	DLPC	340
EcBamA-G807V	4N75, 4C4V	*E. coli*	1100	OM	310

mation (see Fig. 2.2). To resolve the relevance of this kink, we performed a 4.2-μs equilibrium simulation of EcBamA (PDB 4N75), which exhibits the zipped conformation, in an OM model. After 200 ns, the C-terminal end of the β16 strand separated from the β1 strand and curled into the barrel lumen, forming the C-terminal kinked conformation seen in two of the BamA crystal structures (Fig. 2.2A). This conformation persists for the remainder of the simulation. In simulations of other BamA structures, kinking is either maintained (in the case of NgBamA) or forms quickly (within 20 ns in the case of HdBamA), suggesting that the kinked conformation is the more energetically favorable state of the BamA β-barrel. Although HdBamA sometimes exhibits a lower degree of kinking than EcBamA and NgBamA, it does not revert to a zipped state; no more than three hydrogen bonds are maintained between the N- and C-terminal strands in any BamA (Fig. A.2).

2.2.2 Mutation of G807 prevents kink formation

In all simulations, a glycine residue in the C-terminal strand was identified as the hinge point for kinking (Fig. 2.2). To test the significance of kinking, we carried out mutagenesis experiments focused on the hinge residue in EcBamA, G807. Mutation of the glycine to alanine, valine, and phenylalanine did not produce abnormal growth phenotypes in our standard assays with and without arabinose (Figs. 2.3A, B), just as we have observed previously [21]. However, when we plated these mutants on LB-agar plates containing only the antibiotics vancomycin or rifampicin, we observed significant differences in antibi-

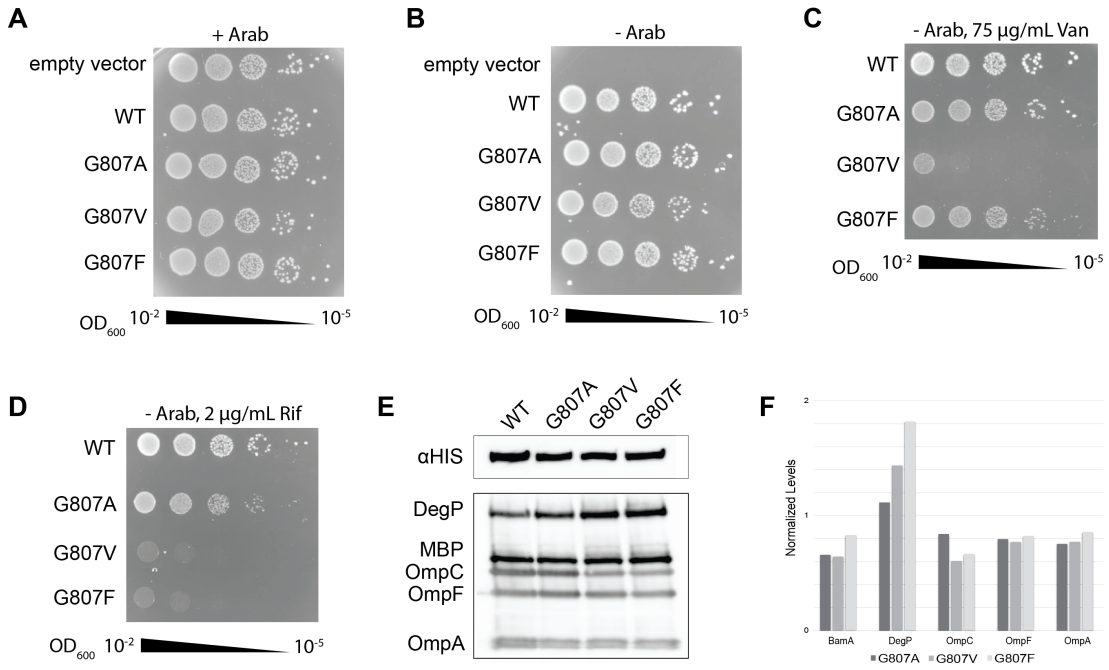

Figure 2.3: Plate growth assays with EcBamA G807 mutants. (A,B) Wild type EcBamA, empty pRSF-1b vector and the G807 mutants were transformed into JCM-166 cells and serial diluted (10^{-2} to 10^{-6}) onto LB-agar plates (A) with and (B) without arabinose. (C,D) The wild type and G807 mutants were investigated further by plating them in the absence of arabinose, but in the presence of either (C) vancomycin (75 μg/mL) or (D) rifampicin (2 μg/mL). (E,F) Expression levels of mutant constructs. Representative experiments are shown from assays performed in triplicate.

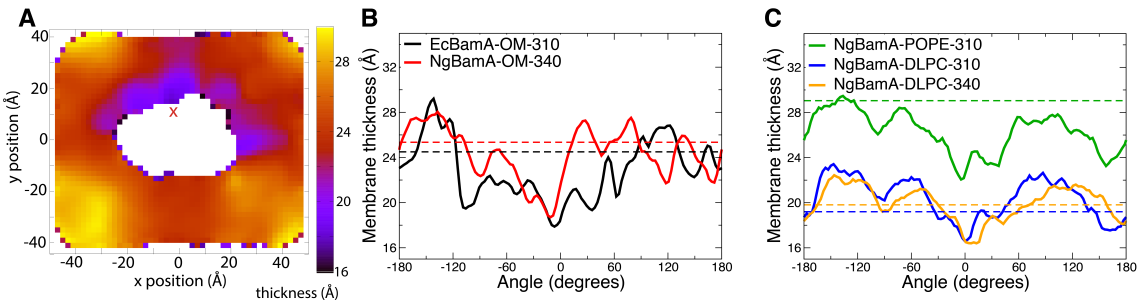

Figure 2.4: Membrane thinning near the N/C-terminal seam. (A) Average membrane hydrophobic thickness around EcBamA over 4.2 μs of simulation in an asymmetric OM model. The red "X" marks the location of the EcBamA seam. See Fig. S4 for additional systems. (B, C) Average membrane thickness within 10 Å of BamA as a function of angle for all five systems. The average angle of the β1 backbone center-of-mass has been set as the zero point. Each system exhibits a dip in membrane thickness near the seam (0°). The average thickness of each membrane is shown for each system as a dotted line.

otic susceptibility for the G807V and G807F mutants. In the presence of vancomycin (75 μg/mL), little to no change in susceptibility was observed for the G807A mutant, compared to WT BamA; however, changes were observed for the other mutants with the most substantial being G807V (Fig. 2.3C). In the presence of rifampicin (2 μg/mL), susceptibility was observed for all the mutants with the most extensive being both the G807V and G807F mutants (Fig. 2.3D). To determine if mutations of this type alter kink formation, we made the G807V mutation *in silico* and observed a persistent zipped conformation over 1 μs (Fig. 2.2A). Together, these results indicate that flexibility along the kink of the C-terminal strand is important for the function of BamA.

2.2.3 Development of membrane defects

Thanks in part to the C-terminal kink, the hydrophobic thickness of the BamA barrel is especially low on the N/C-terminal side (as much as 11 Å thinner; see Fig. A.3). Previous MD simulations of the NgBamA structure showed that this decreased hydrophobic thickness results in a destabilized membrane region [20], which has been proposed to play a role in priming the membrane for OMP insertion [31, 20, 27]. We also observe membrane

thinning near the BamA seam in all simulations performed here, including that of EcBamA in the OM model (Fig. 2.4). The largest decrease in thickness compared to the average (7.0 Å) is demonstrated by NgBamA-POPE-310, with both OM systems being just slightly less (6.6 Å). The smallest decrease is seen in the DLPC membranes (2.6 Å for NgBamA-DLPC-310 and 3.2 Å for NgBamA-DLPC-340), which are already very thin on average ($\sim$20 Å). While the thinning is most consistent and pronounced near the seam, there is also some membrane thinning in other areas, which may be helpful for insertion of large OMPs.

2.2.4 Opening of a lateral gate at the N/C-terminal seam

One of the most unexpected observations in previous BamA simulations is the existence of a lateral gate [20, 21]. Previous equilibrium simulations on the μs time scale displayed spontaneous, repeated separation and closure of the N- and C-terminal strands, albeit in a symmetric DMPE membrane. For comparison, we have examined lateral gate formation in a variety of membrane environments including an OM model. In our simulations, strand separation was observed for NgBamA in DLPC at 310 K and at 340 K, but not in POPE at 310 K (Fig. 2.5D). We also performed 3.1 μs of equilibrium simulation of NgBamA in an OM model at 340 K. At a few points in this simulation, we observed transient separation of the N- and C-terminal strands, despite the stiffness of the OM [72] (Fig. 2.5). However, the simulation was performed at a higher than physiological temperature (340 K), which could be partially responsible for lateral gate opening on the stated time scale. We did not observe gating for EcBamA in the OM model for over 4.2 μs of simulation at 310 K, although the strand separation value was dynamic, nearly crossing the 10-Å threshold at one instance (around 1 μs). It also maintains a lower number of hydrogen bonds than the crystal structure (3 vs. 8; see Fig. A.2). In all equilibrium simulations, a negative correlation between N/C-terminal strand separation and membrane thickness was observed (Fig. B.2), suggesting that gate opening may enhance defects in the membrane.

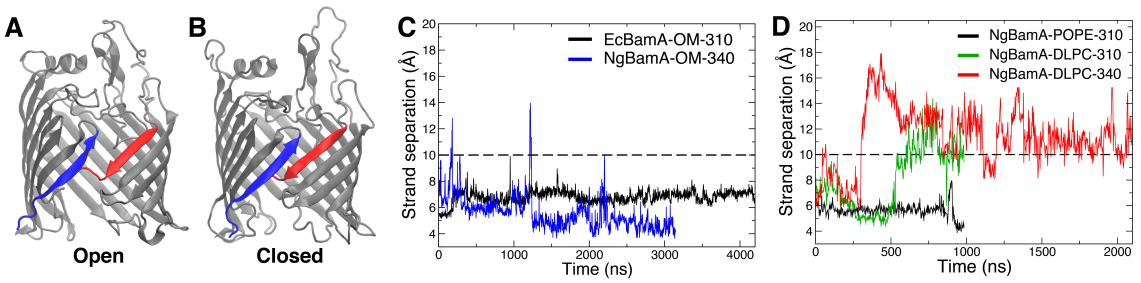

Figure 2.5: (A,B) Snapshots of the (A) maximum strand separation in NgBamA-OM-340 to illustrate the open conformation (around 200 ns) and (B) a low level of strand separation to illustrate the closed conformation (around 550 ns). (C) Strand separation vs. time for BamA in an OM model. Lateral-gate strand separation occurs for NgBamA near 200 ns and again around 1200 ns. (D) Strand separation vs. time for NgBamA in symmetric bilayer systems. Lateral gate separation was observed for DLPC bilayer simulations at 340 K (red) and 310 K (green) but not for POPE at 310 K (black).

2.3 PMF Calculations

To further investigate the factors influencing the stability of the N/C-terminal seam of BamA, we used the replica-exchange umbrella sampling (REUS) technique to calculate the potential of mean force (PMF) for lateral gate opening. BamA from two species, *E. coli* and *N. gonorrhoeae*, as well as FhaC, a homolog with a different function from *B. pertussis* [74], were modified to produce a total of ten unique systems (see Table 2.2). A POPE bilayer was used instead of the stiffer OM [72] to focus on differences between proteins. Most of the systems are discussed in Appendix B, with the focus below on those that were run in the both kinked and zipped conformations.

2.3.1 Energetics of gate opening for EcBamA and FhaC

As a first step in addressing the energetic landscape of lateral gate opening, we calculated the PMF vs. strand separation for BamA from *E. coli* (PDB: 4N75) [20] as well as for FhaC from *B. pertussis* (PDB: 4QKY) [74]. FhaC was chosen as a control system since it is a member of the same protein family (Omp85), contains many structural similarities, and was previously demonstrated to possess a stable β1-β16 interface [20]. Calculated PMFs for EcBamA-WT-z and FhaC-WT-z (nomenclature detailed in Table 2.2) are shown

Table 2.2: Summary of free-energy calculations performed for this study. The labels are given as *(protein)-(modification)-(C-terminal strand conformation)*. For the modification label, WT stands for wild type, "FG" and "BG" stand for FhaC-gate and EcBamA-gate replacement, respectively. "ΔP5" and "ΔL6" stand for deletion of P5 and L6, respectively. The final element of the label, which is either a "z" or a "k", indicates whether the C-terminal strand started in the zipped or kinked conformation, respectively. Unless otherwise indicated, all systems contain a single POTRA domain (P5 for BamA and P2 for FhaC).

Label	PDB	Species	Modification	Start Conform.
EcBamA-WT-z	4N75, 4C4V	*E. coli*	Wild type	zipped
EcBamA-FG-z	4N75, 4C4V	*E. coli*	FhaC gate	zipped
FhaC-WT-z	4QKY	*B. pertussis*	Wild type	zipped
FhaC-BG-z	4QKY	*B. pertussis*	EcBamA gate	zipped
EcBamA-ΔP5-z	4N75	*E. coli*	P5 deletion	zipped
EcBamA-ΔL6-z	4N75, 4C4V	*E. coli*	L6 deletion	zipped
EcBamA-WT-k	4N75, 4C4V	*E. coli*	Wild type	kinked
EcBamA-ΔP5-k	4N75	*E. coli*	P5 deletion	kinked
EcBamA-ΔL6-k	4N75, 4C4V	*E. coli*	L6 deletion	kinked
NgBamA-ΔP5-k	4K3B	*N. gonorrhoeae*	P5 deletion	kinked

in Fig. 2.6. The PMF of lateral gate opening for EcBamA was found to be significantly lower (by 5–10 kcal/mol) than that of FhaC at equivalent degrees of separation.

2.3.2 C-terminal kink formation reduces gate-opening energy

One of the major differences between the EcBamA and NgBamA crystal structures is that in NgBamA, the C-terminal strand already possesses a kinked conformation where the β1–β16 connection is weaker, with only two hydrogen bonds holding the strands together [20]. To assess the role of C-terminal kinking on lateral-gate-opening energy, we calculated the PMF of lateral gate opening starting from the kinked NgBamA structure. This calculation yielded significantly lower PMF values with a relatively flat profile around the closed state (Fig. 2.6). However, the energy difference between kinked NgBamA and zipped EcBamA is 10-15 kcal/mol, which is within the expected range, considering an additional 6 to 8 hydrogen bonds must be broken in the zipped EcBamA lateral gate, each with ~ 1.6 kcal/mol per hydrogen bond [75] (Figs. B.6 and B.7). To better understand the role that kink formation plays in lateral gate opening energetics, we repeated the EcBamA PMF calculation for

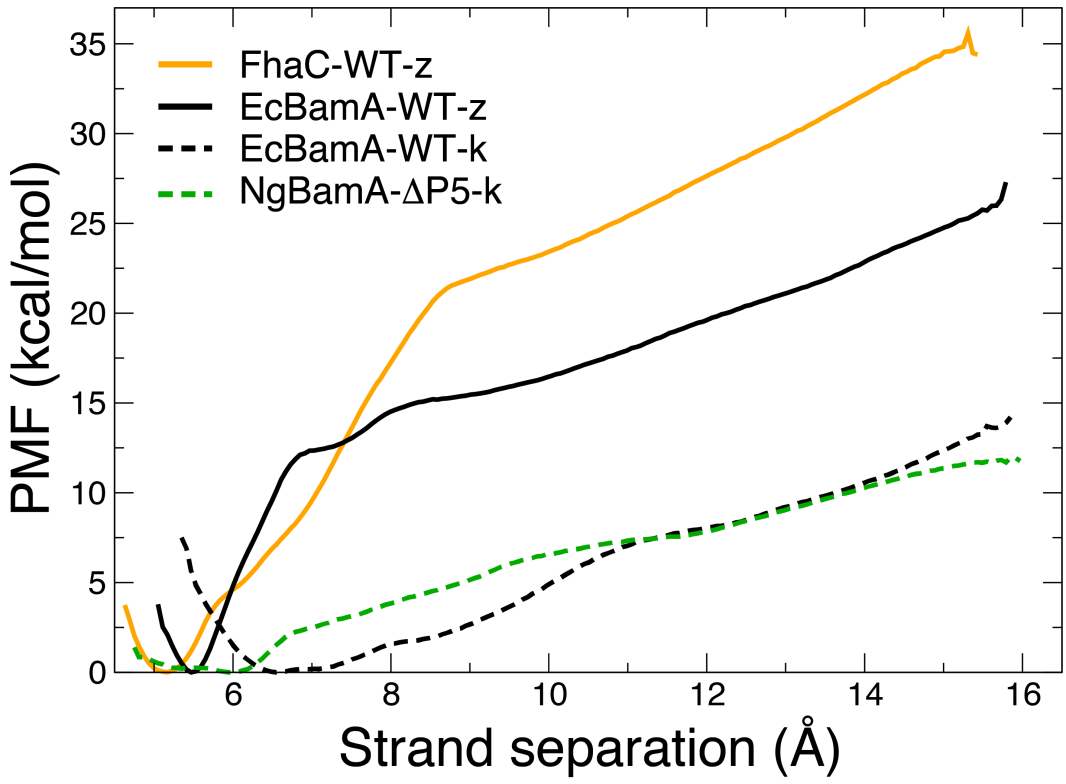

Figure 2.6: PMFs for lateral-gate opening at N/C-terminal seam. PMFs for all BamA variants are lower than that for FhaC. PMFs for kinked starting states (dashed lines) are lower than those for zipped starting states (solid lines). See Figs. B.3 and B.4 for additional PMFs and Fig. B.5 for convergence and statistical error.

a modified starting state in which the C-terminal strand was already kinked. We observed a significant decrease in PMF values, as expected from the NgBamA PMF. However, the kinked EcBamA PMF also displays a deeper energetic well than that of NgBamA with a minimum shifted by about 1.0 Å with respect to the zipped EcBamA PMF (Fig. 2.6).

2.3.3 Determinants of β-barrel stiffness

To determine the role of the β-barrel beyond the N/C-terminal strands, we calculated the average slope of the PMFs from 10 Å to 15 Å (Fig. B.8), i.e., beyond where the barrel-seam strands interact. FhaC variants presented the highest slopes at $\sim$2.2 kcal/mol·Å whereas BamA presents a range of 1-2 kcal/mol·Å, suggesting that not only is the seam of BamA adapted for opening but possibly its entire β-barrel as well. The lowest slopes were consistently found for BamA constructs missing P5 (1 kcal/mol·Å). P5 interacts with a varying number of periplasmic loops depending on its position, and, thus, it may serve as a switch to modulate BamA's ability to open laterally. This is particularly interesting in light of more recent results on the role of P5 gleaned in chapter 3.

2.3.4 Mean first passage time of gate opening

To reconcile the PMF calculations with observations in equilibrium simulations, we determined the mean first passage time (MFPT) of four systems as a function of gate-opening distance (Fig. 2.7). For both zipped states (EcBamA-WT-z and FhaC-WT-z), the MFPT at openings even as low as 7 Å are beyond the accessible simulation time scale. For the kinked states (EcBamA-WT-k and NgBamA-ΔP5-k) on the other hand, the MFPT predicts that openings above the empirical gate-opening cutoff (10 Å) are possible on the μs time scale, as was observed in some of our equilibrium simulations. While we did not observe gate opening for NgBamA-ΔP5-k in a POPE bilayer in 1 μs, this simulation time is just under the MFPT for this system; we expect a simulation 5-10x longer would display transient opening.

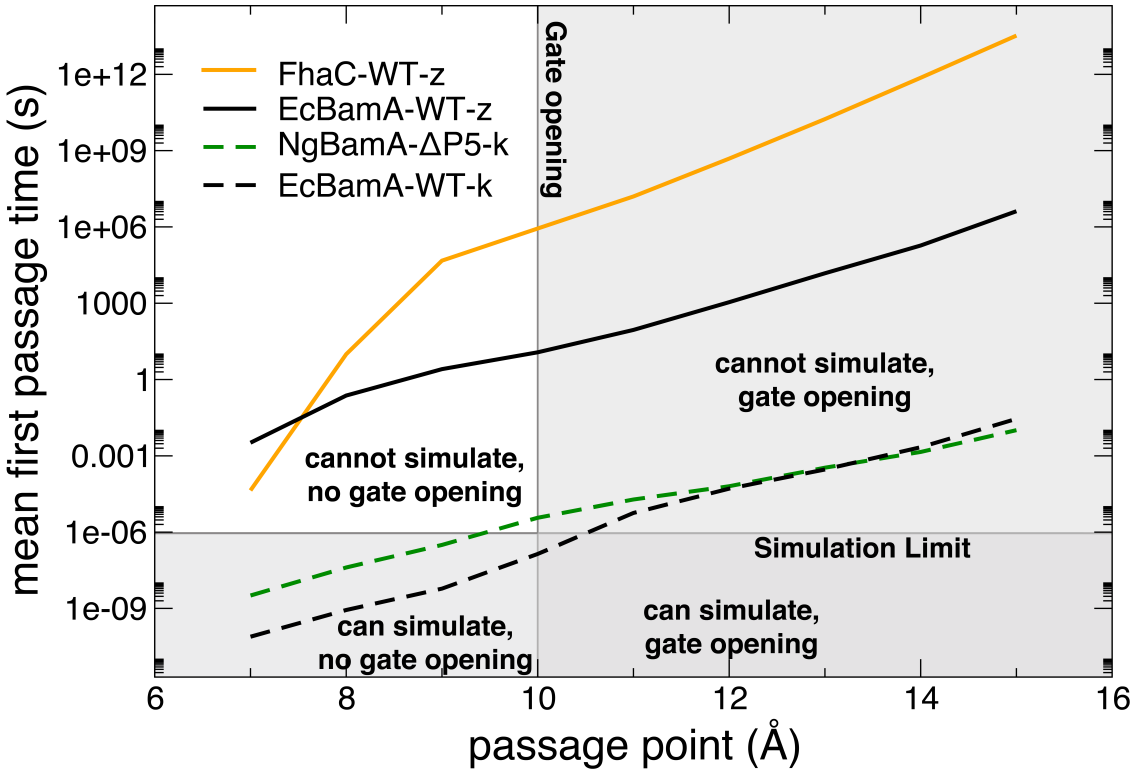

Figure 2.7: Calculated mean first passage times as a function of gate-opening distance [76].

2.3.5 Evidence for gating in TamA

TamA is a BamA homolog implicated in assisting the folding of a subset of OMPs. Due to its similarly to BamA in architecture, it was suspected that TamA possesses a lateral gate as well, but evidence for this feature is absent. We performed PMF calculations of β-barrel seam strand separation for TamA. These calculations revealed the energetic profile of gate opening is very similar to that of BamA in the kinked state, presenting the first evidence supporting that TamA also utilizes a lateral gate to assist in the folding of OMPs (Fig. B.3) [46].

2.4 Conclusion

In this chapter we have discussed our attempts to characterize the molecular determinants of gating in BamA. We determined that membrane thinning induced by a thin hydrophobic band on BamA induces localized membrane thinning OM, POPE, and DLPC membrane environments in a manner proportional to the hydrophobic thickness of the membrane. We also showed that lateral gating exists in OM and DLPC bilayer environments and that a only the kinked conformation of the C-terminal β-strand is viable. Furthermore, we resolved PMF calculations of strand separation to conclude that this C-terminal kink formation was the primary determinant for lateral gating propensity and that only in the presence of the kinked conformation can gating occur on a physiological timescale.

2.4.1 Equilibrium simulations

In order to address the role of the lateral gate in BamA function, we performed a series of equilibrium MD simulations in several membrane environments including an approximation of bacterial OM, a POPE bilayer, and a DLPC bilayer. We also performed a calculation of the energetic landscape associated with the opening of the lateral gate. In our equilibrium simulations, we observed the transition of the C-terminal strand from a zipped to a

kinked conformation but never the reverse transition. In over 11 μs of simulation, we never observed the presence of a stable zipped conformation, casting doubt on its physiological relevance. Mutagenesis experiments also point to the need for a kinked C-terminal strand, as demonstrated by the increase in antibiotic susceptibility when C-terminal strand residue G807 is replaced with either alanine, valine, or phenylalanine (Fig. 2.3). Equilibrium simulations demonstrated that indeed the G807V mutation prevented C-terminal kink formation (Fig. 2.2). Furthermore, we observed opening of the NgBamA lateral gate in several systems, including in a native OM (albeit at 340 K) and in DLPC. Finally, we observed localized membrane thinning due to a hydrophobic mismatch between the membrane and the barrel near the lateral gate. The observed thinning was most prominent for the thicker membranes (OM and POPE) and much less pronounced in the thinner DLPC. In addition to the thinning near the lateral gate, the symmetric membrane systems also demonstrated thinning on the side of the barrel opposite the lateral gate.

2.4.2 PMF calcalations

We calculated the energetic landscape of lateral gate opening for a total of ten systems. For the zipped conformation, EcBamA was shown to possess a lower barrier to opening as compared to a control protein (FhaC) with no suspected lateral gate. The importance of the C-terminal kink formation observed in the equilibrium simulations is echoed in the PMF results; systems that began in a kinked conformation exhibited drastically lower opening energies (10–15 kcal/mol) when compared with zipped wild-type BamA (EcBamA-WT-z). In fact, the importance of the kinked state is further demonstrated by the fact that deletion of two important moieties produce opposite effects on the energy profile depending on whether or not the kink is present. In particular, deletion of loop 6 (L6) and POTRA 5 (P5), result in a decrease of opening energy with respect to zipped wild-type EcBamA but a slight increase with respect to kinked EcBamA (see Appendix B). Any perturbation of the zipped wild-type BamA state translates to a decrease in opening energy. However, the fact

that modifications to the kinked state result in an increase in energy points to the possibility that these moieties have evolved to assist BamA in maintaining its permissive lateral gate. In general, our results point to a crucial role played by the barrel seam. This role supports existing models either as a membrane insertion point and/or as a template for nascent OM proteins.

2.4.3 Outlook

While the present results add to the body of evidence indicating that the formation of a lateral gate plays an important role in the function of BamA, a mechanism consistent with all the present findings has yet to emerge. Recently, striking evidence for a budding model was presented in a tour de force mutation study of the mitochondrial BamA homolog Sam50 [32]. However, another recent study indicated that a disulfide-locked lateral gate still accelerates the insertion of an eight-β-strand OmpX, which runs contrary to a substrate templating mechanism [29]. The narrative that may be emerging is that a single mechanism is insufficient to describe the insertion of all substrates. A different mode may be used depending on the size or makeup of the OMP being inserted. For low-strand-number OMPs, it is possible that they close their barrel prior to insertion [77]; however, for the high-strand-number OMP FimD, the C-terminus inserts prior to the N-terminus [78]. Regardless, membrane thinning, as consistently observed in our simulations, plays a vital role in OMP insertion by significantly lowering the insertion free-energy barrier. We observed a correlation, albeit tenuous, between membrane thinning and lateral gate strand separation (Fig. B.2), which suggests that lateral gating may be to induce further membrane thinning and destabilization, consistent with the passive model. However, it may also be argued that the low level of correlation we observe is evidence that the primary role of lateral gating cannot be to induce membrane thinning. Thus far, none of the existing models have been eliminated; it is even possible that multiple models are correct, depending on the size or makeup of the OMP being inserted.

CHAPTER 3

LIPOPROTEINS ACT TO STABILIZE THE OPEN STATE OF THE BAM COMPLEX

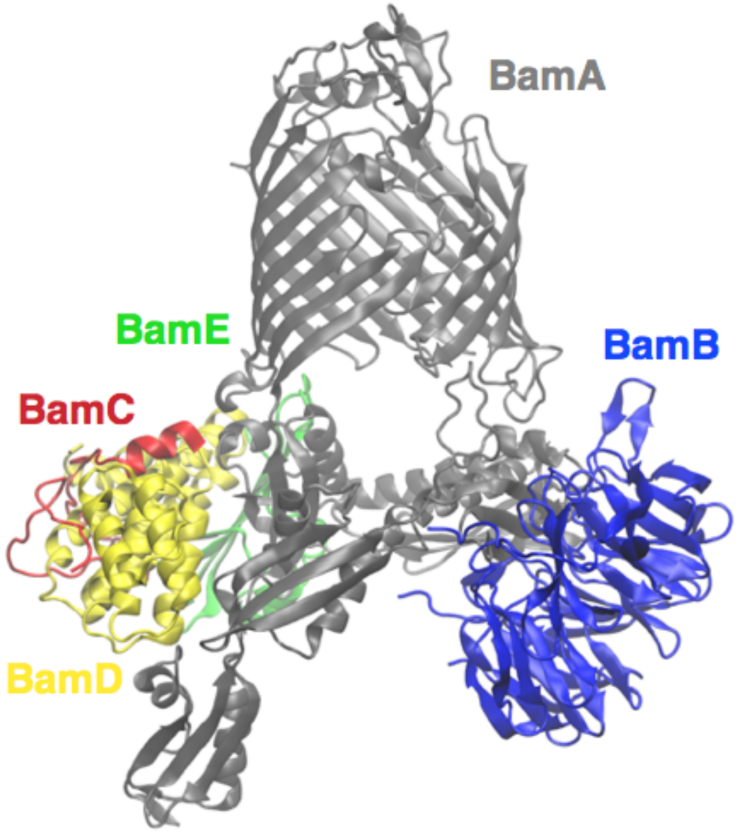

Figure 3.1: The *E. coli* BAM complex from Gu et al. (PDB entry 5D0O) BamA is shown in grey, BamB in blue, BamC in red, BamD in yellow, and BamE in green. The helix grip domains are missing from BamC. BamB and BamD interact directly with BamA, while BamC and BamE interact primarily with BamD.

3.1 Introduction

As noted in a previous section, the outer membrane (OM) in Gram-negative bacteria is asymmetric and populated by a number of outer-membrane proteins (OMPs) with β-barrel

transmembrane domains [14]. The primary machinery responsible for insertion and assembly of OMPs in Gram-negative bacteria has been identified as a five-protein complex called the β-barrel assembly machinery (BAM) [14]. While the exact number of BAM-complex components depends on bacterial species [79, 80], in *E. coli*, the BAM complex is a five-protein assembly. The BAM complex consists of BamA, the central and essential transmembrane unit, along with four accessory lipoproteins, BamB, BamC, BamD, and BamE (Fig. 3.1) [62, 14]. An understanding of how this system accomplishes its significant task has been advanced significantly by the steady release of structures for all its components over the last ten years. The structure of BamB, BamC, and BamD were first published in 2011 [81], while the structure of BamE was published in 2008 [82]. The structure of BamB revealed a β-propeller motif with eight blades and a central pore in what has been called a "doughnut" shape [83]. The structure of BamC consists of an unstructured N-terminal domain (75 to 100 residues) and two structurally similar helix-grip domains, each of which include six β-strands and three α-helices [84, 81, 85]. BamD contains five tetratricopeptide (TPR) domains, each of which consists of two α helices of varying lengths [86, 81, 87]. Crystal structures for BamA periplasmic domains were first released in 2007 [88], but did not exist for the β-barrel domain until 2013 [20]. At its N-terminus, BamA was determined to possess five periplasmic domains called polypeptide transport-associated (POTRA) domains, which have a conserved $\beta\alpha\alpha\beta\beta$ fold and a 16-stranded β-barrel at its C-terminus [89, 20, 90]. In 2016, the first high-resolution structures for the BAM complex, with and without BamB, were released [17, 19, 18, 64].

3.1.1 Simulations of BAM components

Fueled by a number of crystal structures for BAM-complex components released over the course of the last ten years, molecular dynamics simulations have played a critical role in revealing a mechanistic understanding of OMP assembly [20, 21, 91, 19]. Beginning with the release of structures for the β-barrel domain for BamA, simulations revealed several

key features of the dynamics of BAM-complex components. The first of these features was a spontaneous separation between the first and last β-strands (β1 and β16, respectively) on the μs timescale, forming a putative "lateral gate" [20]. To verify the existence and relevance of this gate, cross-linking was performed with disulfide mutagenesis to prevent the gate from opening [21]. This mutation was lethal to bacterial cultures, giving support to the biological existence and importance of the separation event. A second feature revealed in BamA simulations was a destabilized region of the membrane near the strand interface caused by abnormally thin hydrophobic section of the barrel exterior. Together, these features have targeted the gate region as functionally relevant for OMP insertion, although they do not unambiguously establish the actual insertion mechanism. Following the initial simulations of BamA, later MD simulations demonstrated the existence of an exit pore in the extracellular loops above the lateral gate, with crosslinking experiments showing that its opening is required for proper function [21]. It was proposed that this exit pore is necessary to allow the passage of large extracellular loops of nascent OMPs during assembly.

3.1.2 Simulations of BamA

More recently, simulations were used to carry out a systematic study of the POTRA domains of BamA. In this study, Fleming et al. showed that the periplasmic OM surface can bind to the POTRA domains and modulate their conformational flexibility [91]. Based on their findings, they propose that binding to lipoproteins and to the membrane helps the POTRA domains to maintain functionally relevant conformations of the BAM complex. Moreover, due to their amphiphilic nature, β-strand segments of nascent OMPs may find a favorable environment at the interface of the OM inner leaflet and adsorb to the surface. The binding of POTRA domains to this interface may help to arrange these segments into hairpins or β-sheets along the assembly pathway.

3.1.3 Simulations of BAM subcomplexes

Simulations of the full-complex structures released in 2016 have served to broaden an understanding of dynamic features of the complex [19]. The two C-terminal helix-grip domains of BamC were previously suggested to be cell-surface exposed *in vivo*, likely indicating that they are not closely associated with the complex [50]. In all simulations of BAM complex structures, the C-terminal domains of BamC were observed to be the most mobile of all the domains [19]. Likewise, in one of the BamACDE complexes, electron density was only visible for the N-terminal loop of BamC, indicating that the C-terminal region was highly dynamic [19]. The BamACDE and BamABCDE systems were otherwise shown to be stable in simulations [19]. Removal of BamB or BamD caused an increase in mobility, while the removal of BamC had a minimal effect. Gu et al. conclude, based on their simulations and functional studies, that the entire periplasmic part of the complex rotates about the β-barrel domain of BamA, cycling between conformations to somehow assist in OMP assembly [19].

3.1.4 Models for OMP insertion

Inspired in part by the recent structures and simulation results, three prominent models now exist to explain the role of BamA in substrate insertion [31, 15]. The passive model posits that the substrate is inserted directly into the disordered membrane region created by BamA, and otherwise the BamA barrel plays practically no functional role. The luminal folding model asserts that nascent proteins fold entirely inside the lumen of the barrel before exiting through the lateral gate opening. Finally, the hybrid barrel model supposes that the strand separation at the lateral gate creates a β-strand-folding template upon which the strands of the nascent barrel are constructed. The BamA β-barrel grows as each nascent strand is added until the newly formed barrel buds off and is released into the membrane.

OMP insertion model deficiencies

A number of questions and possible shortcomings exist with each of the aforementioned models. The passive model appears to have almost no role for the BamA β-barrel, other than to create a membrane defect. The lumenal folding model would require BamA to accommodate and fold proteins in its lumen, some of which are much larger than BamA itself. In addition, lumenal folding without gate opening would fail to provide an amphiphilic interface to stabilize both the hydrophobic exterior and hydrophilic interior of nascent OMP strands. The hybrid barrel model would provide this amphiphilic interface as well as a template to assist β-sheet formation, but the enormous degree of structural reorganization required to accommodate some OMPs (up to 26-strands [43]) appears untenable on its face [31, 15].

3.1.5 Conformations of the BAM complex

The initial four crystal structures exhibited two main conformations which we will call the closed and open conformations. The two crystal structures which were solved in the absence of BamB exhibited the open conformation, while those which were solved in the presence of BamB exhibited the closed conformation. This correlation between complex conformation and BamB presence led to the hypothesis that BamB binding modulates between these two complex conformations. More specifically, it seemed that the binding of BamB drove the complex into the closed conformation, while unbinding of BamB allowed the complex to take on the open conformation. However, the following year, a cryo-EM structure was released which included BamB, but exhibited the open conformation, upending the previous hypothesis of BamB conformation regulation. In fact, our simulations indicate the BamB acts to stabilize the complex conformation, whether it is closed or open, and when BamB is removed, the open conformation system indicates a significant reversion to the closed conformation.

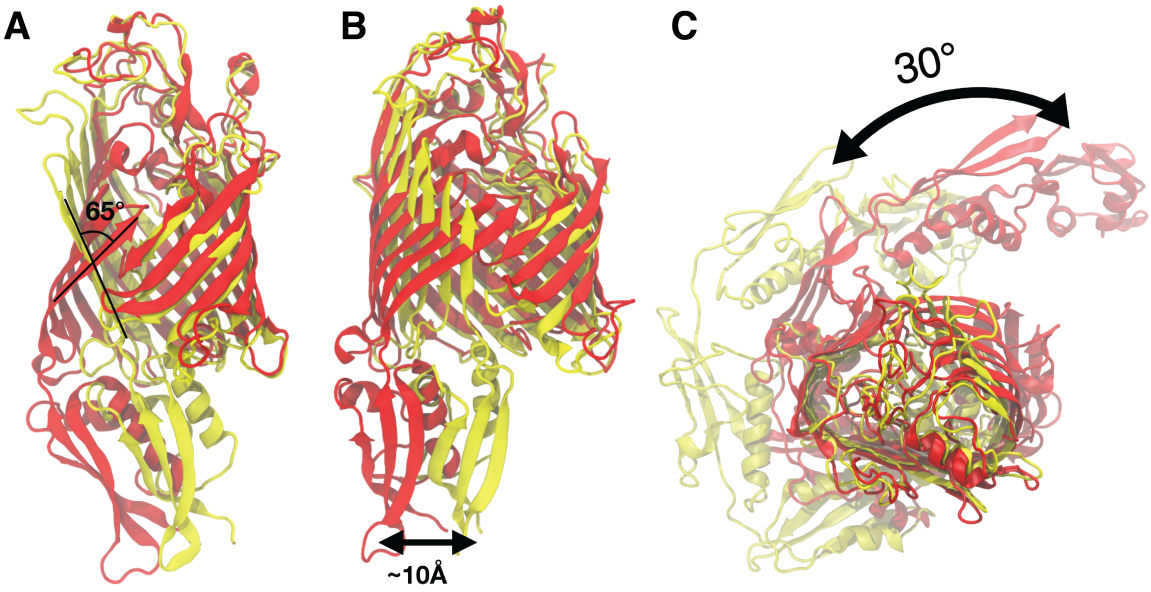

Figure 3.2: Primary features distinguishing the BAM complex conformations highlighted. (A) The lateral gate of the BamA β-barrel is sheared in the open state compared to closed. (B) POTRA5 is positioned directly beneath the BamA β-barrel in the open state, but located further away in the closed state. (C) The accessory proteins and periplasmic domains shift by about 30° counterclockwise in the x-y plane in the open state compared to the closed state.

3.1.6 Features of the BAM complex conformations

In order to discuss the simulation results further, we first need to understand the important features which distinguish the two BAM conformational states. They differ in three principal ways. In the open state, the first four to six N-terminal strands are twisted away from the barrel at the top. This leaves a large hole in the extracellular side of the barrel, with the N-terminal (β1) strand making about a 65° angle with respect to the same strand in the closed conformation (Fig. 3.2A). The second feature is the position of the fifth POTRA domain (P5). As the N-terminal strands twist away at the top in the open conformation, at the bottom they move into the β-barrel, displacing P5 around 10Å to a position directly underneath the BamA β-barrel, completely blocking off access between the barrel interior and the periplasm (Fig. 3.2B). The third feature is that as the barrel opens and P5 moves underneath the barrel, all the the remaining periplasmic domains rotate counter-clockwise by about 30° (Fig. 3.2C).

3.1.7 Model for conformational switching

Based on these features and conformations, our current hypothesis is that random fluctuations of the periplasmic domains or the binding of some chaperone would result in the rotation of those domains which then results in the shift in P5 position and subsequently torques the BamA β-barrel seam into the open conformation, and that this open conformation is supported in order to allow for rapid insertion of substrates. However, many questions remain surrounding the role that these conformations and the accessory proteins play in accelerating the assembly of OMPs. First, are both of these conformations physiologically relevant or perhaps just crystal artifacts? If they are physiologically relevant, what is the role of each of these conformational states? Second, does switching occur between these states in nature? If so, what causes the switching to occur, and what is the timescale of the switching? Third, what is the role played by each of the periplasmic proteins in assisting OMP folding?

3.2 Results

We have attempted to address these questions through the use of molecular dynamics. To do so, we have constructed six simulation systems based on the BAM complex crystal structures and carried out over 13 μs of equilibrium simulation on these systems (Table 3.1). We are also currently involved in resolving the least action pathway between the two conformational states through the use of the string method [92].

Table 3.1: Summary of simulations used for the study of BAM complex dynamics.

Structure	Source	Runs
5D0O	Gu et. al [19]	1012ns, 1004ns
5D0Q	Gu et. al [19]	2106ns, 2006ns
5LJO	Iadanza et. al [64]	1008ns, 1010ns
BamA Only	Based on 5D0Q, BamA Only	1010ns, 1009ns
5D0O w/o BamB	Based on 5D0O without BamB	1003ns, 1006ns
Barrel Only	Based on 5D0Q, Barrel Only	509ns, 510ns

3.2.1 Accessory proteins stabilize the open conformation

The story that has emerged from the analysis of our BAM complex equilibrium simulations is that the accessory proteins act to maintain the BamA β-barrel in the open state. We observe in our simulations that without the accessory proteins, BamA cannot maintain its open state. This open state may be a folding active state stabilized to rapidly fold OMP substrates [19, 93].

3.2.2 Partial complexes do not maintain sheared BamA β-barrel seam

In order to illustrate this observation, we have analyzed the main distinguishing features of the conformational states over the course of our simulations. The first of these is in the angle formed by the first four N-terminal β-strands of the BamA β-barrel. We have computed the vector average of these strands (β1-β4) using the principal component of each strand, and determined the angle it makes with the vector average of the same strands in the closed conformation after alignment. This data is shown over the course of each simulation in Fig. 3.3. The data indicates that the only systems which retain their angle are those which are either in the closed state, or those which contain all BAM complex components. BamA β-barrel only (open), BamA only (open, with P1-P5), and BamACDE (open) all indicate a significant level of seam closing indicative of a reversion to the closed state. Previous studies have indicated a minimal effect on OMP assembly rates due to the deletion of BamE [54] or BamC [58]. While we did not perform these deletions in silico, one would likely expect a higher level of stability in these deletion systems due to these studies and the lower contact area BamE and BamC have with BamA. Our data indicates that BamB plays a significant role in maintaining the BamA β-barrel in the open state and this is consistent with previous studies reporting a significant reduction in OMP assembly rates in the absence of BamB [59]. It seems that the stability of complex formation is in some way compensating for an energetically unfavorable conformation of the BamA β-barrel in the open state.

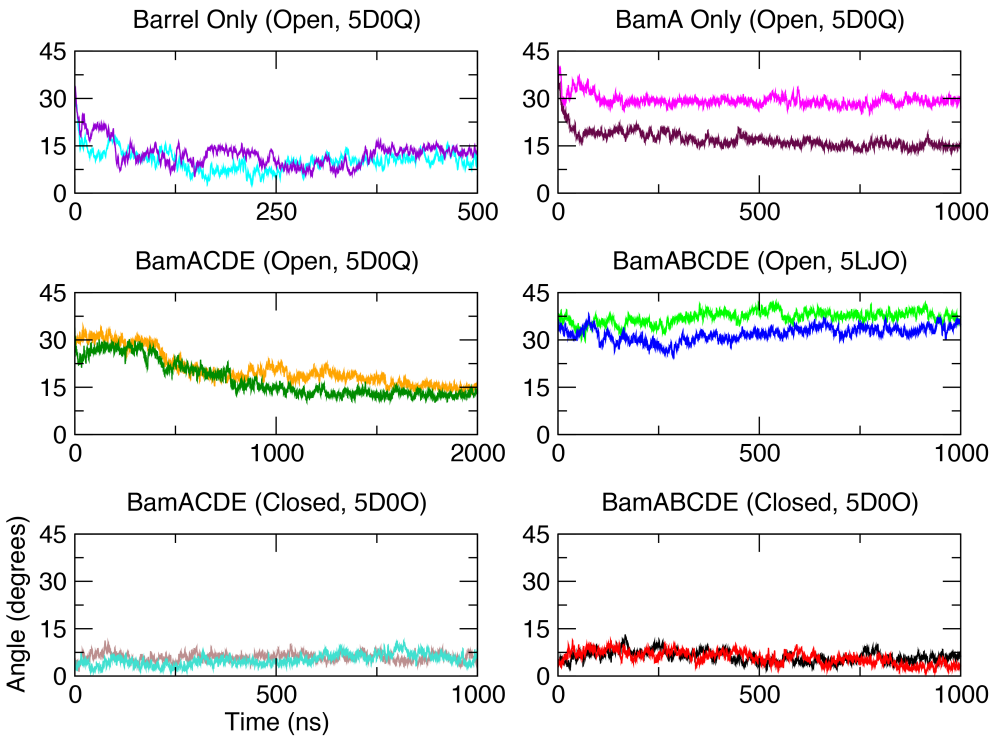

Figure 3.3: Angle of BamA β1-β4 obtained by determining the vector average of the principal axes of each of these strands in the current frame and comparing them to the vector average of the same strands in the closed conformation after alignment. This measurement shows that each of the full complexes retain their starting states, open or closed, but when BamB is deleted, the open state closes, while the closed state remains closed. Closing of the β-barrel lateral gate occurs for both BamA systems which begin in the open state. However, one replica of full BamA failed to close beyond about 30° by perhaps finding a transiently stable open state.

3.2.3 Shifts in POTRA 5 position

The second distinguishing feature of the conformational states we analyzed from our equilibrium simulations is the position of the fifth POTRA domain (P5). To do this we have created a scatter plot of the x- and y-positions of the P5 center of mass for each of the trajectories. Points in the bottom right region of the graph are indicative of the distal position of P5 in the closed state. The points closer to the origin, or on the top left portion of the graph are indicative of the open state where P5 is located directly beneath the BamA β-barrel (Fig. 3.4). P5 for the BamA replica shown to revert to the closed state in Fig. 3.3 contains data points that cross into the spread of the closed states, while the replica which did not close appears to move away from the closed state, perhaps unable to find a path toward the closed state. Deletion of BamB in both the open and closed states seems to move P5 further away from the center, and its position in the opposite state. This may indicate that BamB, while playing a role in stabilizing the complex, also helps to hold the complex in a position more conducive for switching between the two states.

3.2.4 Rotation of the periplasmic domains

In all of our simulations, the periplasmic domains exhibited rotational dynamics with respect to the BamA β-barrel. We have attempted to demonstrate this rotation by plotting the standard deviation ellipses generated from the x- and y- position data of each accessory protein and POTRA domain (Fig. 3.5). These plots demonstrate that while the positions are fairly stable for all closed state systems (Fig. 3.5B and 3.5C), a significant amount of rotation occurred in these domains for both the intact and nearly intact systems in the open state (Fig. 3.5E and 3.5F). Furthermore, BamACDE-open indicates a rotation of all domains toward the closed state positions consistent with data from Fig. 3.3 demonstrating a closing of the gate for these same systems. This suggests that the complex is poorly able to maintain the open state in the absence of BamB and that the closing of the BamA lateral gate is paired with a clockwise rotation of its periplasmic domains.

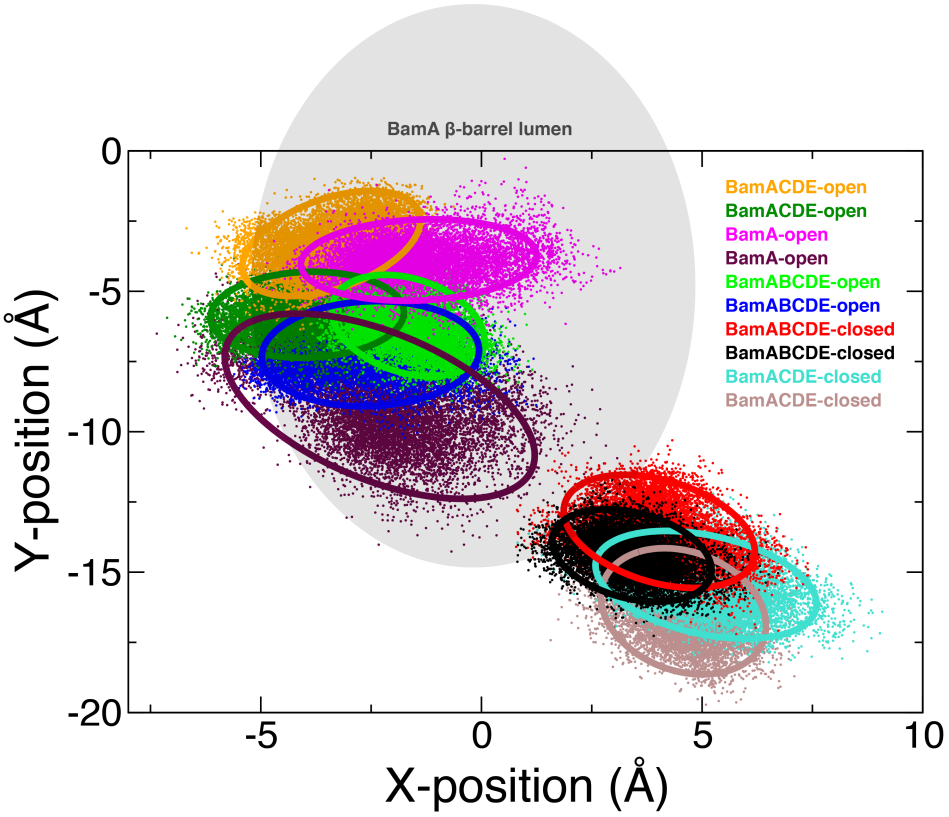

Figure 3.4: Scatter plot of x- and y-position of P5 domain throughout each of the simulations. Standard deviation ellipses are shown to clarify the spread in the data for each system since significant overlap occurs.

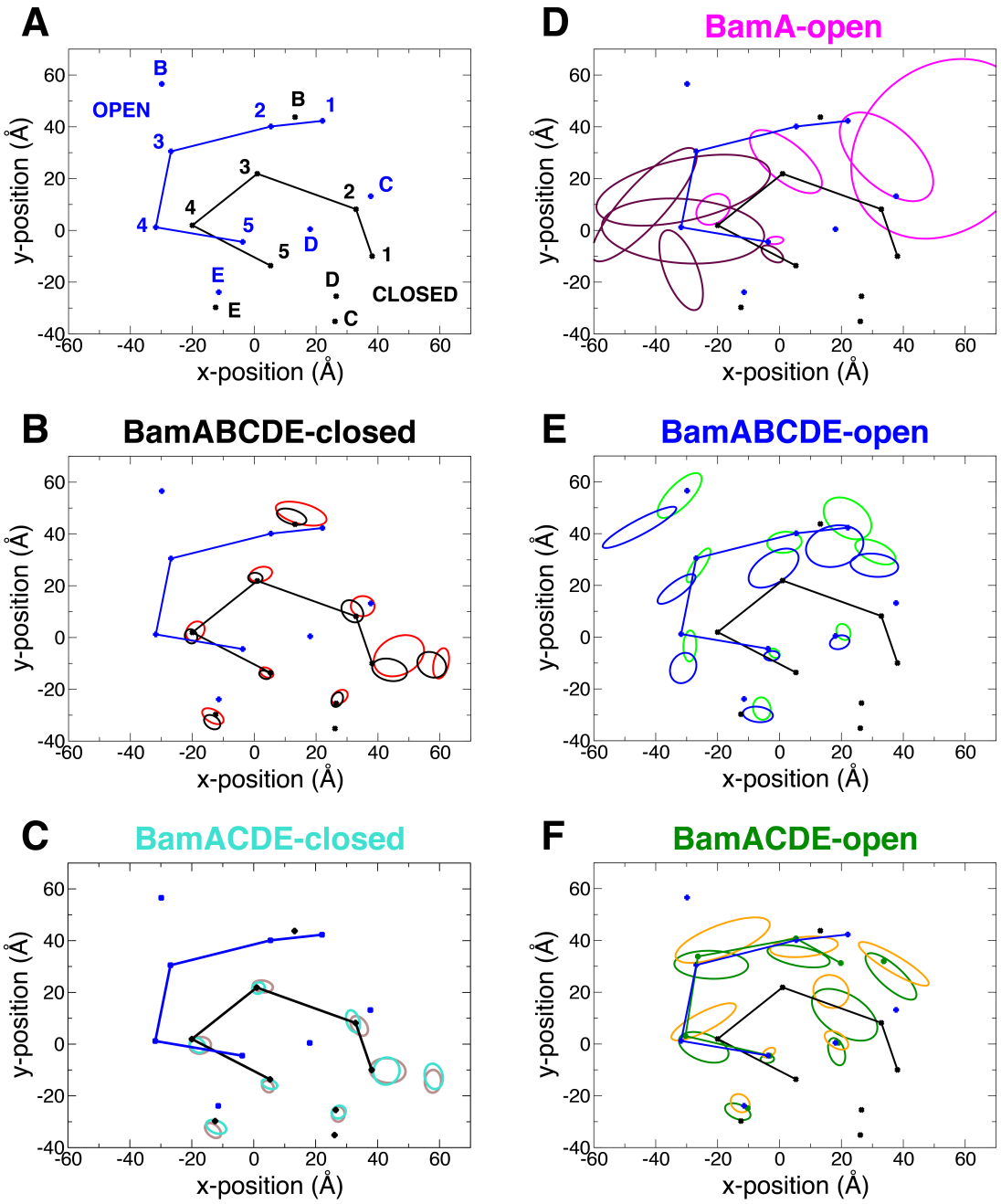

Figure 3.5: Standard deviation ellipses based on the center of mass x- and y- position of all accessory proteins and POTRA domains which illustrate their dyanmic range over the course of the simulation trajectories. (A) A schematic of the positions of the periplasmic domains in the open (blue, PDB: 5LJO) and closed (black, PDB: 5D0O) published structures. All domains in open states (D,E, and F) exhibit a larger dynamic range the the respective domain in the closed position, which is largely expressed as a rotation of these domains with respect to the BamA β-barrel (placed at the origin).

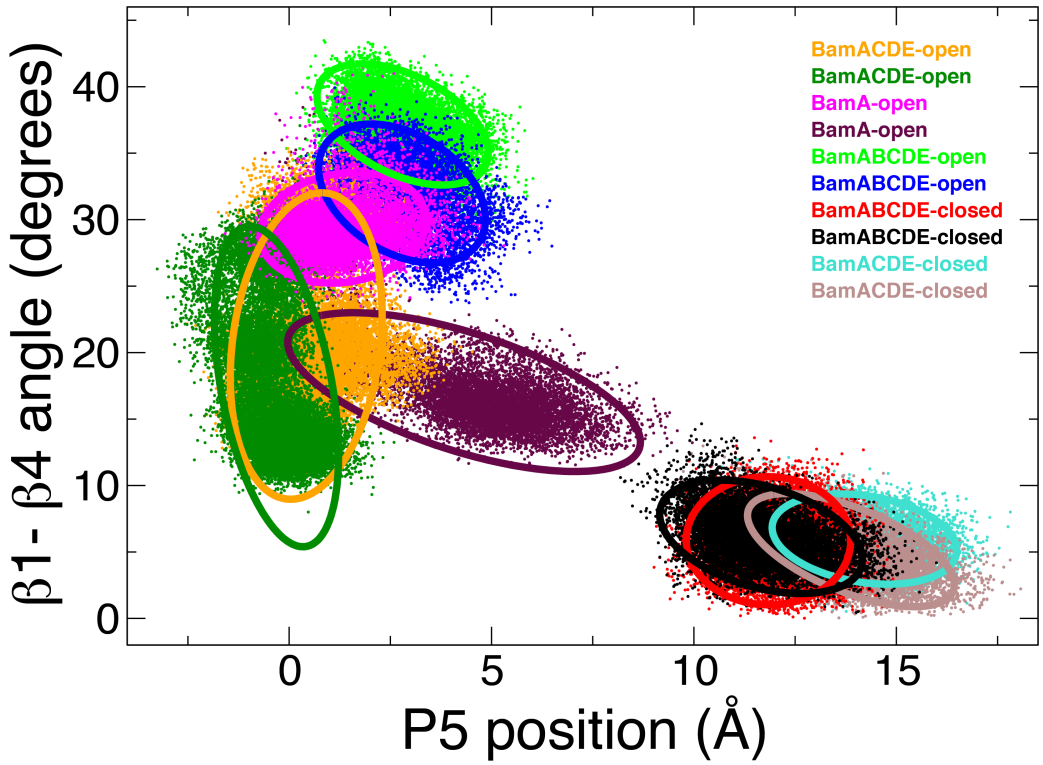

Figure 3.6: Lateral gate angle vs. P5 position. Lateral gate angle is measured as in Fig. 3.3. P5 position was determined by projecting a vector from P5 in the open state to P5 position in the current frame onto the vector between P5 in the open and closed state. With this measurement, P5 is zero in the open state and the distance between P5 between the two states in the closed state. This plot indicates the extent to which a correlation between gate angle and P5 position exists. For most systems, the long axis of the ellipse suggests a negative correlation between the angle and P5 position.

3.2.5 Correlation between key features

We observed a correlation between the lateral gate angle and the P5 position. However it seems to be a nonlinear correlation. P5 is able to move substantially without affecting much of a change in the lateral gate angle and lateral gate angle is able to change substantially without enacting a change on the position of P5 (Fig. 3.6). The long axis of nearly all systems' standard deviation ellipse suggests a negative correlation between lateral gate angle and P5 position, especially for BamA alone.

3.3 Conclusion

An important open question concerning BAM complex function is concerning how the association of BAM complex members assists the BAM complex in folding substrates. In order to determine the roles of the accessory proteins and dynamics of the BAM complex as a whole, we performed equilibrium simulations. The four initial BAM complex crystal structures presented in two main conformations. Those copurified with BamB exhibited the laterally closed state and those without BamB were in the laterally open state. Three main features of the BAM complex can be used to characterize these two conformations: lateral gate angle, POTRA5 position, and rotation of the periplasmic ring. We examined the dynamics of these systems through the lens of these three features. We found that all systems in the open state were much more dynamic than those in the closed state. Furthermore, any system other than the full five-member complex exhibited closing of the lateral gate indicative of reversion to the closed state. Lastly, paired with this closes of the lateral gate, open systems lacking BamB also exhibited a clockwise rotation which would suggest a reversion to the same closed state configuration. One mystery that still remains is this while we observe this indication of closing in the lateral gate angle as well as the periplasmic ring rotation, this change is not reflected in the position of P5, which at the onset we conjectured was the mechanistic link between the periplasmic ring and the lateral gate. This missing link indicates that we need to more carefully examine the dynamics of BamD and its ability to dictate conformational changes directly to the BamA β-barrel without using P5 as a mediator.

CHAPTER 4

ACTIVE FEATURES GOVERNING THE LPTD/E INSERTASE

4.1 Introduction

4.1.1 The cell envelope of Gram-negative bacteria

Gram-negative bacteria are characterized by their unique cell-envelope structure consisting of two lipid membranes. The inner membrane is a symmetric phospholipid bilayer and the outer membrane consists of a phospholipid inner leaflet and an outer leaflet composed of lipopolysaccharide (LPS) molecules [94]. The space between the membranes is host to a large number of proteins as well as the peptidoglycan cell wall and is known as the periplasm. LPS molecules possess a hydrophobic portion called lipid A consisting of around six acyl tails, a core oligosaccharide region of phosphate groups and sugars, and a long O-antigen sugar chain whose composition varies considerably among species [33]. These LPS molecules form an external barrier for Gram-negative bacteria, protecting them from environmental antagonists such as immunity factors and antibiotics.

4.1.2 Assembly of LPS

The assembly of LPS molecules begins at the cytosolic side of the inner membrane where biosynthesis of lipid A is first performed by the Lpx protein family and core oligosaccharide is added by Waa proteins [33, 34, 35]. The partially assembled LPS is flipped across the inner membrane by the ABC transporter MsbA, the O-antigen chain is ligated, and finally transported across the periplasm by the LPS transport (Lpt) machinery. The Lpt machinery is a seven-protein complex consisting of LptA–G [36], all of which are essential [37]. At the inner membrane LptBFG is an ABC transporter which hydrolyzes ATP to transfer LPS from the inner membrane to LptC [38, 39]. LptC, -A, and -D each possess a

Table 4.1: Summary of simulations performed. SfLptDE included β-barrel and N-terminal domain, while PaLptDE included only the β-barrel domain.

name	description	T (K)	membrane	PDB	length (ns)
Sf	S. flexneri	310	DMPE	4Q35	746
Sf-340K	S. flexneri	340	DMPE	4Q35	761
Sf-LPS	LPS in JR	310	DMPE	4Q35	3000
Pa-1	run 1	310	DMPE	5IVA	1540
Pa-2	run 2	310	DMPE	5IVA	485
Pa-340K		340	DMPE	5IVA	720
Pa-lipid	lipid inside	310	DMPE	5IVA	710
Pa-OM-1	Pa	310	OM	5IVA	1530
Pa-OM-2	Pa	310	OM	5IVA	1140

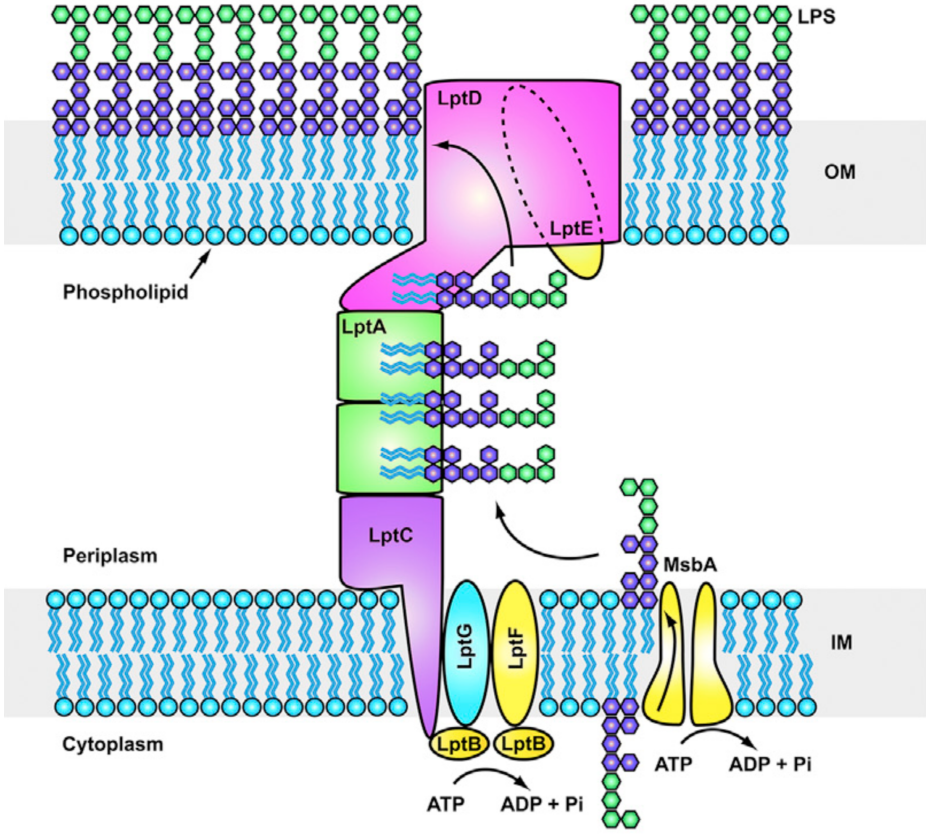

Figure 4.1: The lipopolysaccharide transport system. The Lpt system is made up of seven proteins. LptBFG associate to form an ABC transporter, which extracts LPS from the outer leaflet of the inner membrane, passing it to the single-pass inner membrane protein LptC. The soluble domain of LptC associates with a string of LptA monomers, which in turn associate with the N-terminal domain of LptD to provide a hydrophobic track for LPS to transit the periplasm. LPS is transported across the outer membrane and inserted into the outer leaflet by the LptD/E complex.

β-jellyroll domain with a hydrophobic interior [40, 41]. These three proteins link together with hydrogen bonds along their β-strands to span the periplasmic space and shuttle LPS molecules using interactions between the hydrophobic groove and lipid A tails [42]. Finally, LptD/E is thought to escort LPS to the outer membrane by separating its first (β1) and last (β26) stands.

4.1.3 Features of LptD/E

Crystal structures of LptD, first released in 2014, revealed a 26-strand β-barrel domain and an N-terminal β-jelly roll domain. At the proximal tip of the N-terminal domain are several hydrophobic residues in a region predicted to embed into the outer membrane. This putative LPS insertion site is also near the barrel seam between β1 and β26. Simulations at a high negative pressure by Dong et al. [43] demonstrated a separation between β1 and β26, which was posited to act as the gate though which LPS would pass. Due to the existing structural and simulation data, the prevailing model for the role of LptD/E is that it facilitates the passage of LPS molecules to the outer membrane by accepting them at the N-terminal jelly roll and then ushering them through the separation between β1 and β26. However, many questions surrounding the molecular details of this insertion process remain.

4.1.4 Simulations of LptD/E

In order to better clarify the insertion process, we have performed over 10 μs of equilibrium simulations of two LptDE crystal structures (PDB 4Q35 and 5IVA) in both a symmetric phospholipid bilayer (DMPE) and an outer membrane (OM) model. Our simulations have indicated several characteristic transformations which may be vital to the function of LptDE and act as prerequisites for lateral gate opening and substrate ushering.

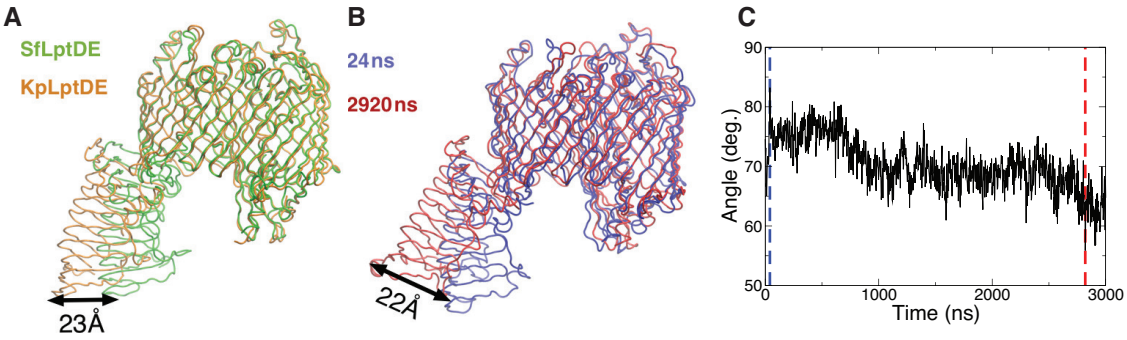

Figure 4.2: (A) Alignment of SfLptDE and KpLptDE demonstrating the difference between their N-terminal domain positions. (B) Snapshots at 24 ns and 2920 ns illustrating the similar range of N-terminal domain motion observed in our simulations. (C) COM distance relative to frame 0 of 11 distal C_α atoms (resid 52 to 62) in the N-terminal domain vs. time. For reference, location of snapshots used in center figure are highlighted in blue and red.

4.2 Results

4.2.1 Proline residues destabilize β-barrel seam

A special property of proline residues is that they resist the formation of secondary structure. We performed simulations that indicated three proline residues near the β-barrel seam of LptD act to destabilize the interface between strands β1 and β26. Our collaborators also performed mutations which indicated that the deletion of these prolines is detrimental to bacteria (Fig. 4.3) [47].

4.2.2 N-terminal domain flexibility

A flexible hinge may be required between the N-terminal "jelly-roll" domain of LptD and the C-terminal barrel. Comparison of the full-length SfLptDE [41] and KpLptDE structures reveals a 23 Å shift in the distal end of the N-terminal domains. Equilibrium simulations of SfLptDE produced N-terminal domain fluctuations of a similar magnitude over the course of our 3 μs simulation trajectory. To date, two crystal structures have been published of LptD which include the N-terminal β-jelly-roll domain, KpLptDE (PDB: 5IV9) [47] and SfLptDE (PDB 4Q35)[41]. An alignment of the β-barrels of these structures reveals that

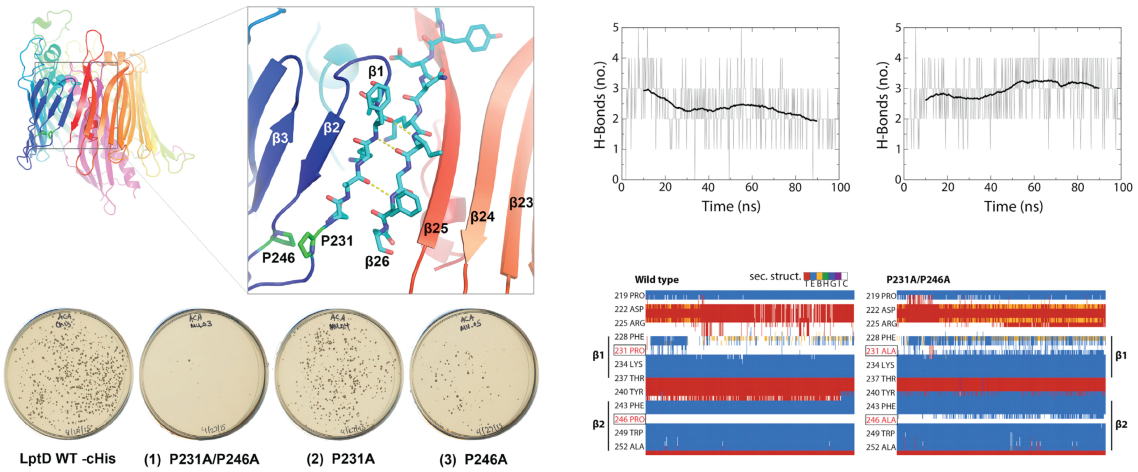

Figure 4.3: Three proline residues destabilize LptD lateral gate. (top left) Lateral gate and position of P246 and P231 labeled. (bottom left) Double mutant (P231A/P246A) causes significant growth defects, while each of the single mutants are viable. To demonstrate this growth defect is due to the instability caused by the proline residues we mutated P246 and P231 to alanine and showed an increase in the number of lateral gate hydrogen bonds (top right) and secondary structure (bottom right).

the N-terminal domain is shifted by about 23 Å at the distal end suggesting a high degree of conformational flexibility exists in this domain. This flexibility may exist to maintain the integrity of the periplasm-spanning complex by withstanding relative motions of the inner and outer membrane components. However, differences in crystal structures alone could be due to sequence-dependent characteristics of the protein or differences in artifacts of crystal packing between the structures. In our 3 μs trajectory of SfLptDE we observed considerable dynamics of the N-terminal domain resulting in a maximal displacement of about 22 Å at the distal end in agreement with the differences observed in crystal structures (Fig. 4.2). Witnessing this feature in molecular dynamics simulation adds credence to the assumption that a flexible hinge exists between the LptD β-barrel and the LptD β-jelly-roll domain.

4.2.3 Membrane environment affects loop dynamics and secondary structure

To address the effect of the outer membrane environment on LptDE, we performed over 2 μs of equilibrium simulations for PaLptDE in both DMPE and OM. In these simula-

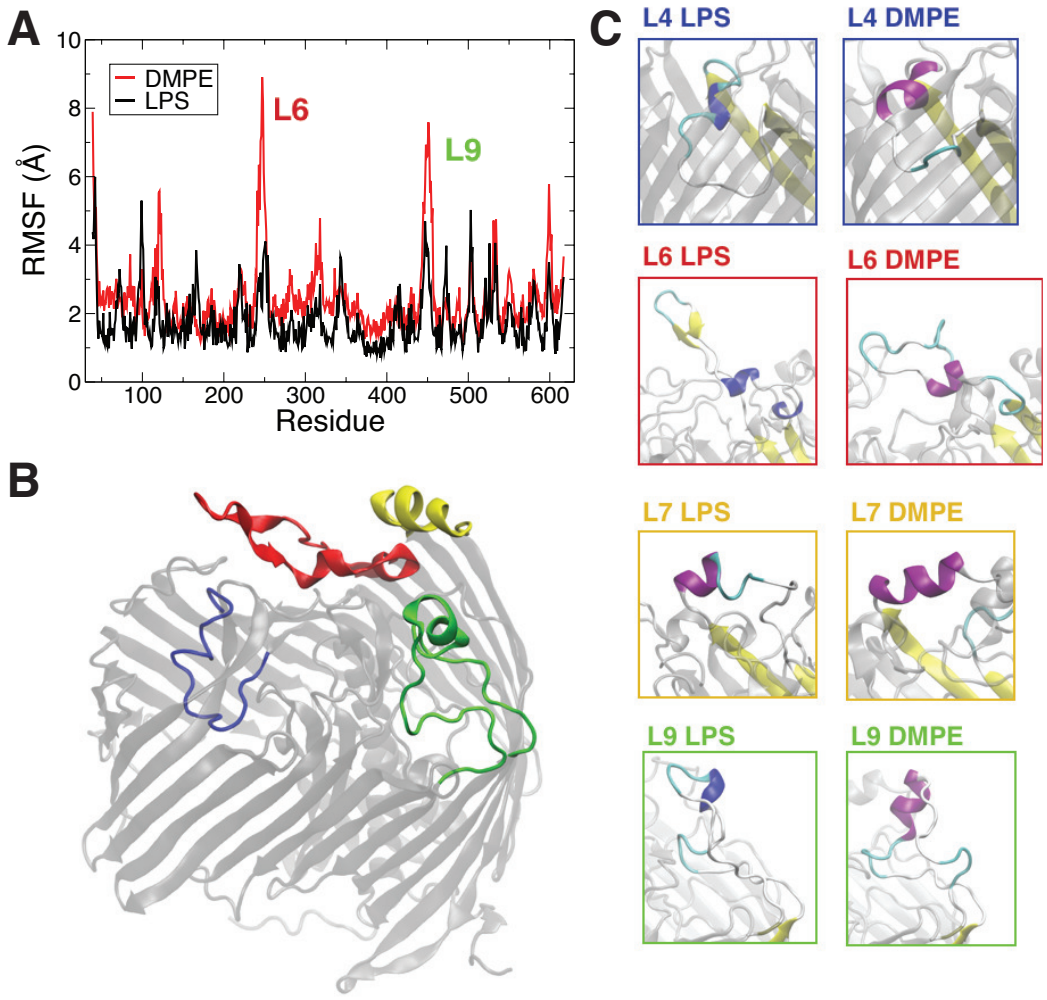

Figure 4.4: Secondary structure and RMSF differences. Significantly higher RMSF can be observed in the OM system for the extracellular loops, especially in L6 and L9. Prominent secondary structure differences exist in L4, L6, L7 and L9. For L4, a 3_{10}-helix forms in OM whereas the same region forms an α-helix in DMPE. In L6, a β-hairpin is formed in OM which is unstable in DMPE.

tions we observed significant secondary structure and RMSF differences. Overall, a higher RMSF was noted for the DMPE system, especially in the extracellular loops. Significant secondary structure differences could be seen in extracellular loops L4, L6, L7, and L9 (Fig. 4.4). Pseudomonas species posses abnormally large O-antigens, which makes it particularly interesting to look at the effect of the OM environment for their native proteins [47].

4.2.4 Lateral gate switch

Between the β-jelly roll hydrophobic groove and the putative lateral gate which opens for substrate insertion are two periplasmic loops. These two loops are shown to be interacting in the SfLptDE structure as if to block the passage of substrate, while in the StLptDE (PDB: 4N4R) [43] structure the loops are not interacting as if to permit substrate passage (Fig. 4.5) [95]. Over the course of our 3 μs equilibrium simulation we observe a switch-like behavior between these two loops where the distance between them visits what seems to be two discreet states possibly corresponding to open and closed (Fig. 4.5).

4.3 Conclusion

The results presented here paint a picture of the key dynamical features that may be required along the pathway of LPS insertion by LptDE. Our data indicates that the N-terminal jelly-roll domain which delivers LPS to LptDE possesses a flexible hinge to facilitate cohesion of the trans-periplasmic complex. Upon presentation of the substrate, there is a switch in the luminal loops which likely initiates the insertion cascade. Second, mobility of L4 allows LptDE to prepare the lumen for passage of the oligosaccharide region. Finally, interactions between extracellular loops and the highly polar moieties of the LPS molecules allow LptDE to remain in an insertion-competent state by stabilizing the secondary structure and mobility of the loops.

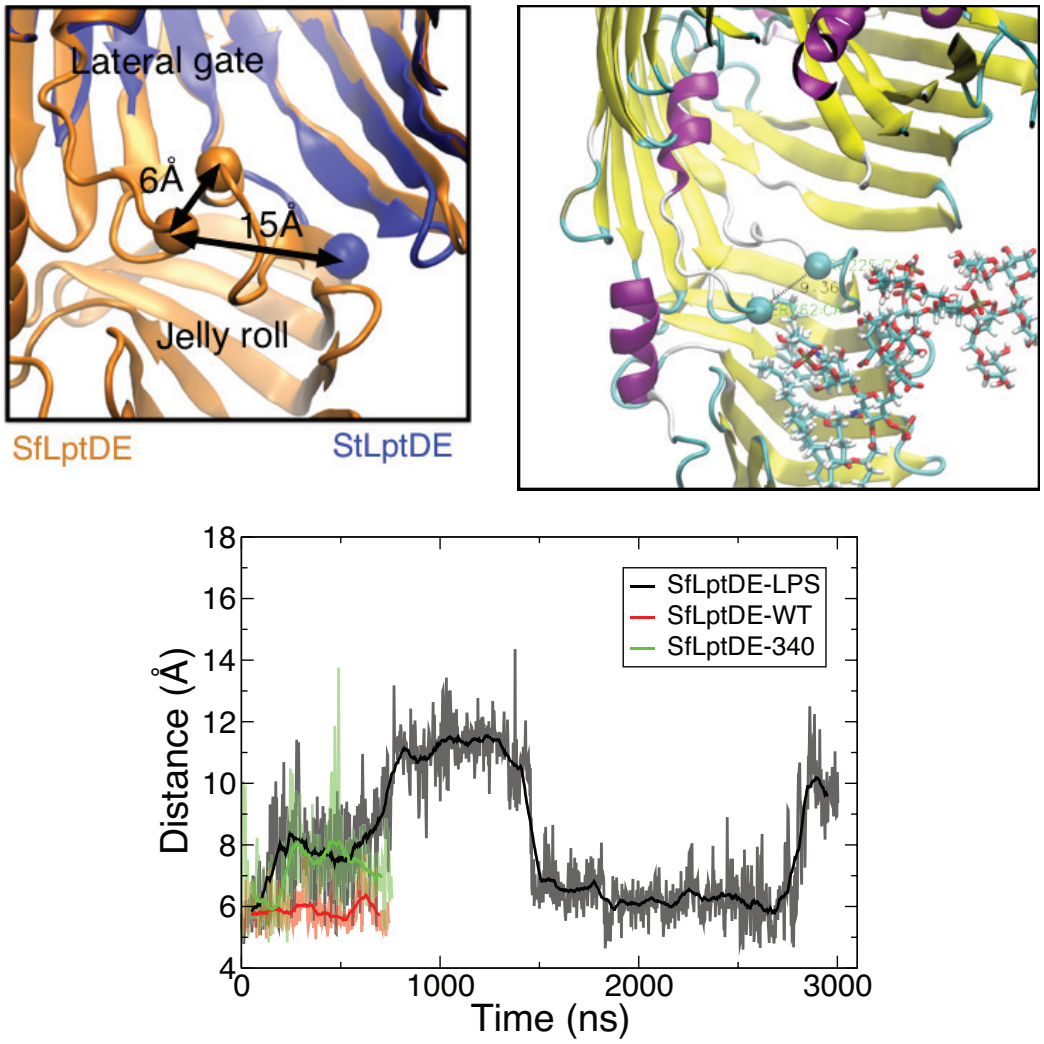

Figure 4.5: Distance between luminal loops (C_α of R225 and S762) demonstrating putative gating region near barrel seam.

CHAPTER 5
CONCLUSION

In this thesis we have discussed novel contributions to the understanding of two key protein systems involved in transport and construction of the Gram-negative bacterial cell envelope. In Chapter 2 we presented evidence that a C-terminal kink is required for lateral gate opening to occur in BamA, and that a key hinge residue, G807 plays a crucial role in the formation of this kink. In Chapter 3 we discussed the dynamics of the full 5-member BAM complex in the presence and absence of the key member BamB. We noted significantly increased dynamics in the BAM open state when compared to the closed state. This is reflected in three main metrics, the angle of the lateral gate N-terminal strands, the position of POTRA 5, and the angle of the periplasmic domains in the x-y plane. Our results also indicate that a change in lateral gate angle is correlated to both P5 position and accessory domain angle, providing evidence that concerted dynamics exist within these features to transition between the open and closed states. Finally, in Chapter 4 we discussed our insights into the lateral-gating based molecular transport of another key outer membrane component, LPS by the outer membrane protein LptD. We revealed the presence of a switch near the lateral gate which we observed to be active only in the presence of a LPS substrate. We also revealed that the presence of an LPS substrate in the N-terminal jelly roll domain to increase the equilibrium distance between the LptD gate strands. Furthermore, our free energy calculations indicated that the presence of this substrate also significantly reduced the barrier for gate opening. We did not observe gating for LptD at equilibrium, but our free-energy calculations indicated that adding the energy of ATP hydrolysis at the inner membrane would bring lower the energy such that gating at equilibrium could be achieved. Through this thesis we discovered key features of two imperative molecular transporters of outer membrane components that both depend on a lateral gating feature.

Appendices

APPENDIX A

METHODS

A.1 Molecular Dynamics Simulations

All simulations are classical, atomistic molecular dynamics that use the molecular simulation program, NAMD [96]. NAMD is developed by Klaus Schulten, director of the NIH Center for Macromolecular Modeling and Bioinformatics at the University of Illinois, Urbana-Champaign, and is freely available to download. For nearly all simulations, the latest iteration of the CHARMM force field, CHARMM36, were be used. All simulations use a 2 fs time step. Short-range interactions were cut off at 12Å as is typically done for the CHARMM force field [97]. Long-range electrostatic interactions was computed using the particle-mesh Ewald (PME) method [98]. All bonds involving hydrogen atoms are kept rigid. As recommended for membrane simulations using CHARMM36, a force-based switching function instead of a potential-based one was used for van der Waals interactions between 10 and 12Å [97].

A.2 Replica Exchange Umbrella Sampling (REMD-US)

Computation of potentials of mean force (PMFs) was proposed for various systems throughout this proposal. PMF is a quantity closely related to the free energy along a given reaction coordinate. In order to compute PMFs, an efficient variant of umbrella sampling, REMD-US, was used [99, 100]. In umbrella sampling (US), as applied here, a given reaction coordinate, e.g., the center of mass distance between lateral gate stand atoms, is divided into a set of closely spaced windows and then restrained using a harmonic potential in each window. The fluctuations about the restrained positions are monitored over time and the resulting histograms are then combined using the weighted histogram analysis method

(WHAM) to produce the PMF [101, 102, 103]. Replica exchange facilitates the rapid exploration of conformational space by permitting neighboring windows to periodically swap coordinates [99, 100].

A.3 Adaptive Biasing Forces (ABF)

Adaptive biasing forces (ABF) is another technique for calculating PMFs which was used throughout this work [104, 105, 106]. In this work ABF was used primarily to drive conformational changes in the lateral gate of BamA. ABF is better suited to these projects than other means of inducing these changes like targeted molecular dynamics (TMD), or steered molecular dynamics (SMD) because it allows for the reaction coordinate to evolve in a quasi-equilibrium during estimation of the free-energy profile. In ABF, the forces applied to induce a transformation are of the same magnitude as the forces experienced by random fluctuations along the reaction coordinate. The ABF method has been efficiently implemented in NAMD [96].

A.4 Targeted Molecular Dynamics (TMD)

Targeted molecular dynamics (TMD) is a technique by which conformational change in a molecular dynamics simulation can be induced [107]. This is accomplished by guiding a subset of atoms toward a 'target' structure by means of steering forces. RMS distance between the current coordinates and the time-dependent target structure is computed at each timestep, where the time-dependent target structure is a linear evolution from the starting state to the final state. The force applied to the atom selection derives from the potential given by

$$U_{TMD} = \frac{1}{2}\frac{k}{N}[RMS(t) - RMS^*(t)]^2 \tag{A.1}$$

Where $RMS(t)$ is the current RMS distance to the target coordinates and $RMS^*(t)$ is the RMS distance from the time-dependent target structure to the final target coordinates.

A.5 Free energy of lateral gate opening

All PMFs demonstrated in the preliminary data section were calculated using the Replica Exchange Umbrella Sampling technique. Each of these simulations was carried out on 20 replicas spaced 0.5Å apart. Center of mass distance between atom selections in each of the gate strands was used as a reaction coordinate for the procedure. These selections included seven C_α atoms and their respective H_α from each strand. All simulations were carried out to 20 ns per window.

A.5.1 MFPT Calculation

In order to calculate the mean first passage times from the PMFs, we utilized a result from Szabo et al. [76]:

$$\int_{x_0}^{b} dx \, \frac{e^{\beta U(x)}}{D(x)} \int_{a}^{x} dy \, e^{-\beta U(y)} \tag{A.2}$$

where $U(x)$ is the PMF; $D(x)$ is the position-dependent diffusion coefficient; a is a reflective barrier, which we chose to be 5 Å; and b is the chosen passage point, here the gate-opening distance. Diffusion coefficients along the REUS trajectory were determined using the generalized Langevin equation approach implemented in ACFCalculator from Gaalswyk et al. [108]. The correlation functions related to the friction produced by the environment were used to calculate the position-dependent diffusivity and were determined by running 1-ns simulations with a harmonic potential at the center of each REUS window for each system, recording the position at every 2-fs time step.

A.5.2 System construction

The *E. coli* BamA system (EcBamA-WT-z) was constructed using residues 344 to 426 (P5) of PDB 4C4V and residues 427 to 810 (β-barrel) of crystal structure PDB: 4N75. The original system had dimensions of 94×78×124 Å which included 17,326 water molecules, 155 POPE phospholipid molecules, 68 potassium and 49 chloride ions for a total system

size of 78,610 atoms. Additionally, a disulphide bond was created between CYS 690 and 700 and P5 was transformed to match the conformation exhibited in the crystal structure PDB: 4K3B.

The *N. gonorrhoeae* BamA system was constructed with residues 417 to 792 (β-barrel domain) of crystal structure PDB: 4K3B. The original system had dimensions of $100\times90\times110$ Å which included 18,114 water molecules, 204 POPE phospholipid molecules, 51 potassium and 62 chloride ions for a total system size of 85,650 atoms. THR743 was added manually since it was missing from the crystal structure.

The *B. pertussis* FhaC system was constructed with residues 6 to 554 (P5 and β-barrel) by joining together several segments from crystal structure PDBs: 2QDZ and 4QKY. Residues 384 to 397 and 476 to 482 were inserted manually since these residues were missing in both crystal structures. During construction, special attention was made toward preserving the updated L6 conformation. ASP269 was protonated based on its pKa value as determined by propKa [109]. The original system had dimensions $96\times94\times124$ Å which included 21,533 water molecules, 209 POPE phospholipid molecules, 61 potassium and 81 chloride ions for a total system size of 97,927 atoms.

After construction, each of the systems was minimized for 10,000 steps and then equilibrated first by releasing system components sequentially (lipid tails for 1.5 ns, everything except protein for 1.5 ns, everything except protein backbone for 1.5 ns). Each system was then equilibrated unrestrained (55 ns for the *E. coli* BamA system, 20 ns for the NgBamA system, and 20 ns for the FhaC system). The end state from this equilibration was used as the closed state for each system.

A.5.3 Modified systems

ABF was applied using as a reaction coordinate the center-of-mass distance between an atom group in each of the $\beta1$ and $\beta16$ stands flanking the lateral gate. The C_α and H_α atoms in seven residues of each strand were included in these atom groups (427 to 433 and

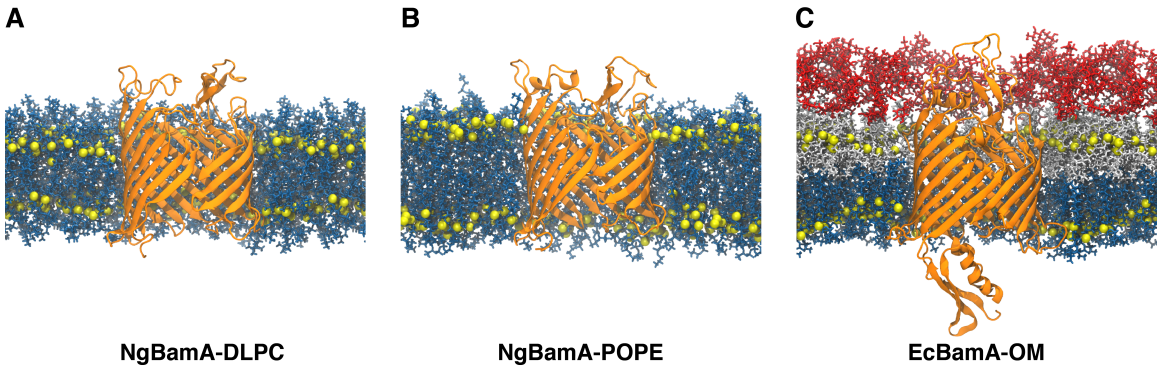

Figure A.1: Systems used for equilibrium simulations. (A) NgBamA in DLPC, (B) NgBamA in POPE, and (C) EcBamA in OM (NgBamA in OM is not shown). Protein is shown as orange ribbons; C2 (and C4 for OM) atoms which delineate the hydrophobic region, are shown as yellow spheres; phospholipids are shown as blue sticks; and lipid A and core oligosaccharide regions of LPS are shown in white and red, respectively.

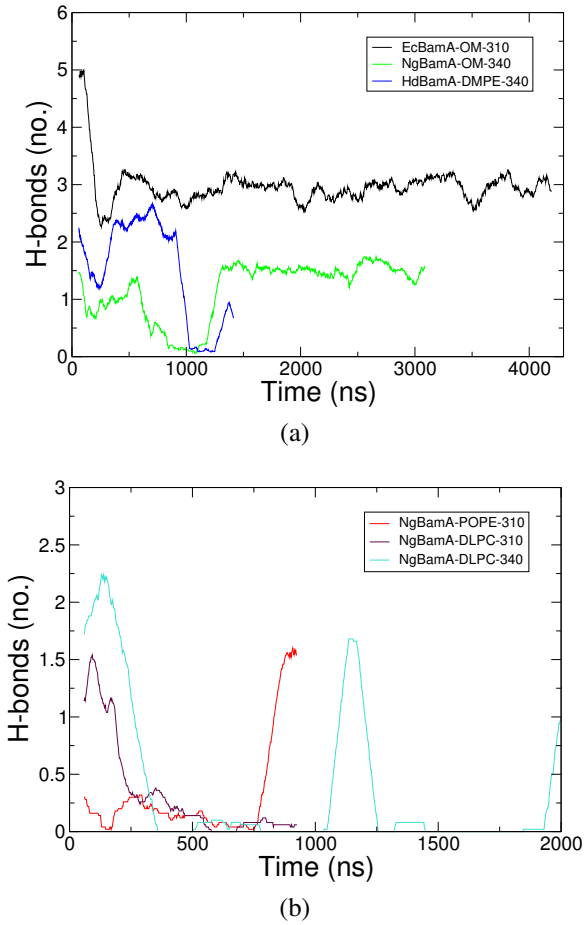

Figure A.2: Gate hydrogen bonds for equilibrium simulations

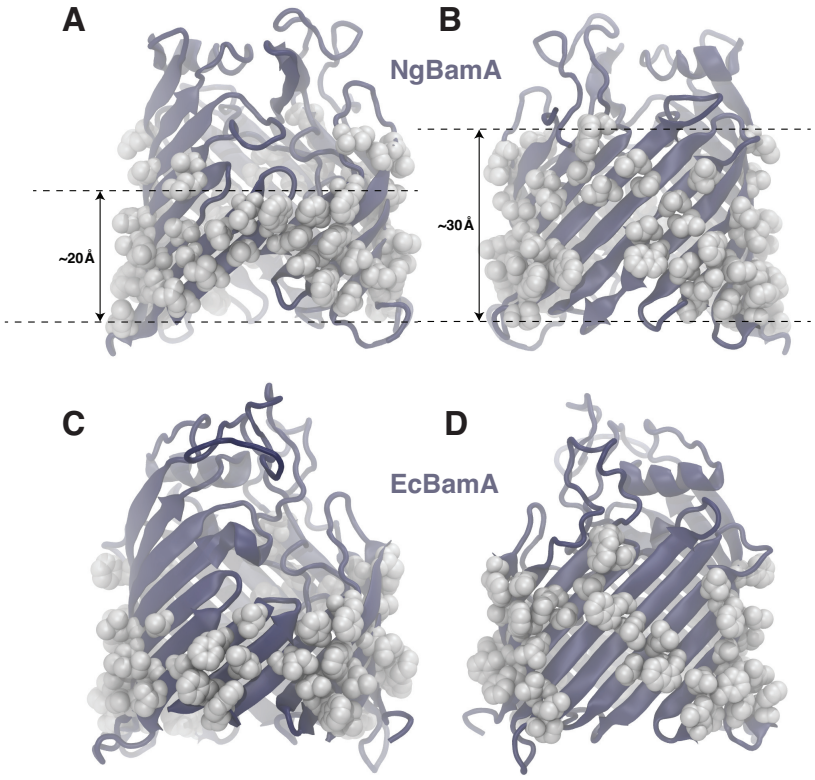

Figure A.3: Hydrophobic residues on the (A, C) lateral-gate and (B, D) opposite sides of the BamA β-barrel domain showing the difference in hydrophobic thickness (A, B; 4K3B; C, D; 4N75). A thin hydrophobic region can also be seen on the opposite side of the barrel causes membrane thinning in our symmetric membrane simulations (Fig. B.1)

804 to 810 for EcBamA, 427 to 433 and 786 to 792 for NgBamA, and 212 to 218 and 548 to 554 for FhaC). The initial opening was carried out with 20 ns of ABF simulation. In order to normalize the open-gate conformation across models, an additional 20-ns relaxation simulation was performed in which colvars restraints were applied, preventing pairwise distances between C_α atoms in opposite strands of the same group from falling below 13 Å. The final state from this relaxation procedure was used as the open state for each system.

Six additional systems were generated by modifying the EcBamA-WT-z system. EcBamA-FG-z, EcBamA-ΔP5-z, and EcBamA-ΔL6-z were produced by first performing in situ modification directly to the open and closed states generated for EcBamA-WT-z, equilibrating each independently for 10 ns (with colvars restraints to keep the open state from closing) and then interpolating between the equilibrated, modified states using a 20-ns targeted MD simulation. The modification for EcBamA-FG-z was that residues 426 to 434 and 802 to 810 were mutated to the corresponding residues in FhaC (211 to 219 and 546 to 554). The modifications for EcBamA-ΔP5-z and EcBamA-ΔL6-z were that residues 344 to 424 (P5) and 654 to 669 (L6) were deleted, respectively. Kinked analogs of all zipped EcBamA systems (EcBamA-WT-k, EcBamA-ΔP5-k, and EcBamA-ΔL6-k) were constructed using a nearly identical procedure, except that the closed reference state was taken from the EcBamA-310-OM equilibrium simulation shortly after the formation of the C-terminal kink.

One additional system was generated by modifying the FhaC-WT-z system. FhaC-BG-z was constructed by directly modifying residues 211 to 219 and 546 to 554 in β-strands 1 and 16 to the corresponding residues in EcBamA (426 to 434 and 802 to 810). After performing the modifications on the open and closed states independently, each was equilibrated for 10 ns.

In order to seed the initial windows of the Replica Exchange Umbrella Sampling (REUS) procedure, 20 ns of targeted molecular dynamics (TMD) simulation was used to interpolate between the closed and open states constructed as detailed above. Selections used for the

TMD procedure were C_α and H_α atoms of residues 426 to 434 and 802 to 810 in EcBamA, 426 to 434 and 784 to 792 in NgBamA, and 211 to 219 and 546 to 554 in FhaC.

APPENDIX B

SUPPLEMENTAL RESULTS

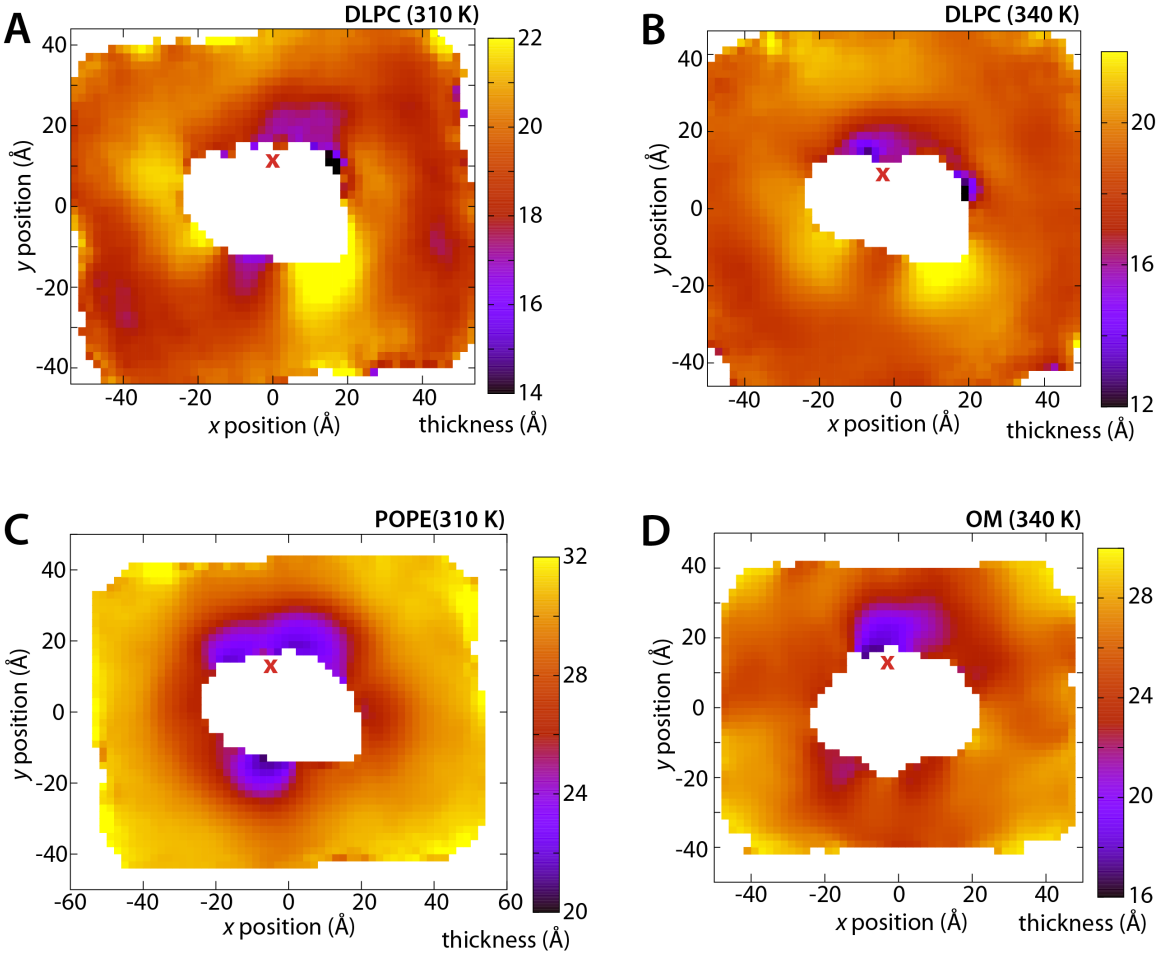

Figure B.1: Two-dimensional membrane thickness calculation for the remainder of the equilibrium simulations. Prominent regions of membrane thinning can be observed near the lateral gate (red "X"), as well as on the opposite side of the protein, especially in the symmetric membrane systems.

B.1 PMF Calculations

Modifying gate strands reduces opening energy. After verifying that the lateral gate opening energy of EcBamA was indeed lower than that of FhaC, we built two modified

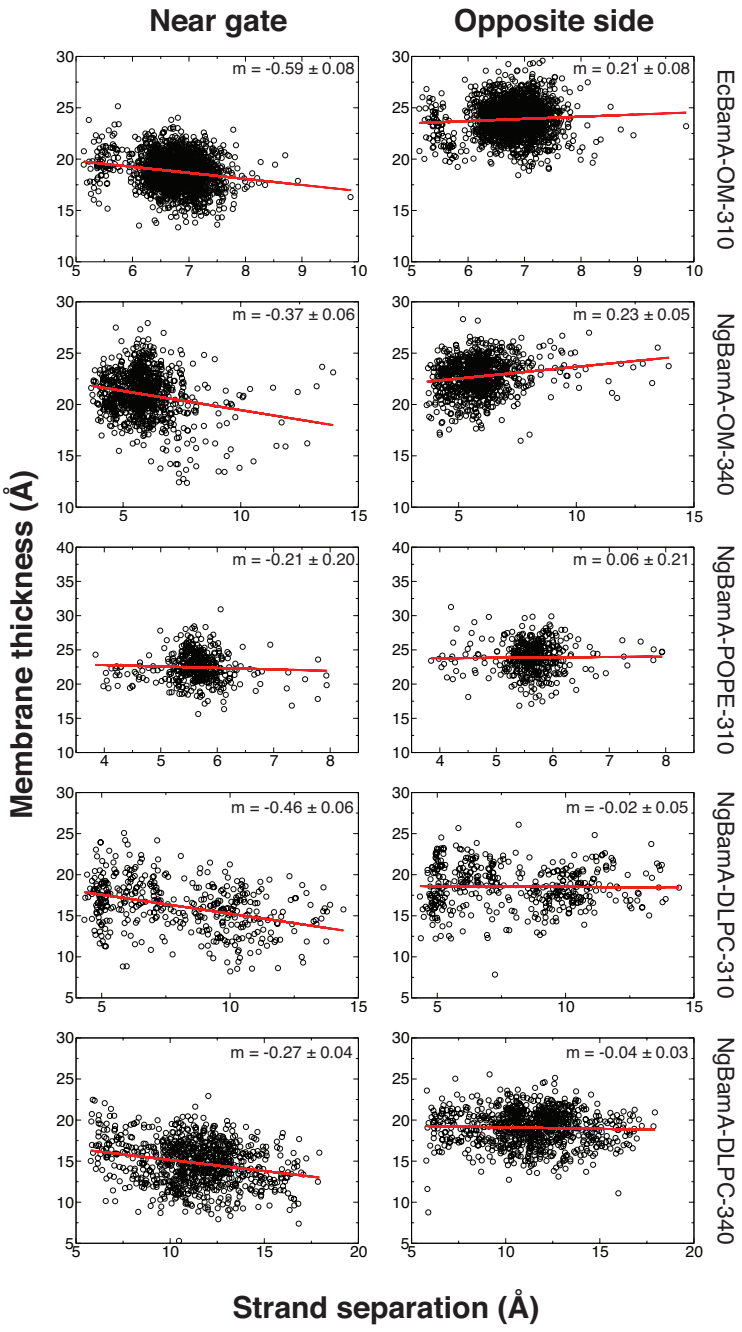

Figure B.2: For each equilibrium trajectory, membrane thickness vs. lateral gate strand separation is shown for lipids near the lateral gate (left), and as a control, on the opposite side of the β-barrel (right). Linear regression demonstrates a negative correlation between membrane thickness and strand separation exists for each of the trajectories (slope shown in top right of each panel). This supports a possibility that lateral gate opening acts to exacerbate membrane thinning and is consistent with the passive model. As reported elsewhere in this thesis, the strand separation was calculated as the center of mass distance between the β1 and β16 strands using C_α and H_α from residues 427 to 433 and 786 to 792 for NgBamA and 427 to 433 and 804 to 810 for EcBamA.

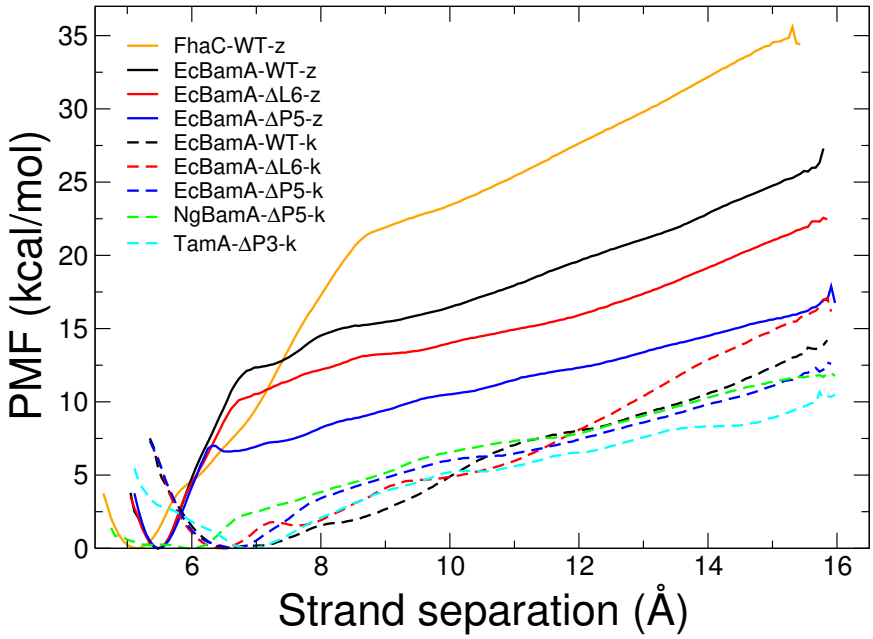

Figure B.3: PMFs for lateral-gate opening at N-C junction. PMFs for all BamA variants are lower than that for FhaC. For the zipped-C-terminal-strand PMFs (solid lines), deletion of L6 (red) produces a slight decrease in opening energy, whereas deletion of P5 results in a similar energetic profile near the minimum PMF value, but a sharp transition to a lower slope at around 6.5 Å separation. PMF values for kinked starting states (dashed) are all lower than their zipped counterparts, and while the effect is less dramatic, deletion of the L6 (red) and P5 (blue) moieties both result in a slight increase in opening energy, as opposed to the decrease seen for the zipped deletions.

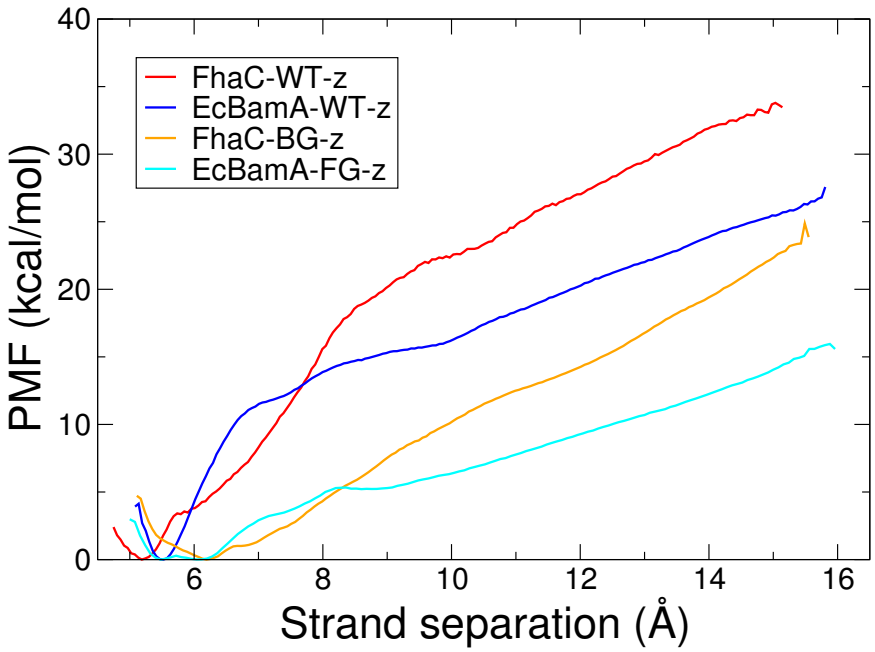

Figure B.4: Lateral gate separation PMFs for β-barrels with fully zipped C-terminal strands. FhaC-WT-z (red) possesses a greater opening energy than EcBamA-WT-z (black). Both lateral gate mutant systems (FhaC-BG-z in green and BamA-FG-z in blue) open at a lower energy than their respective wild types; however, their opening energies are ordered by their β-barrel identity rather than their lateral-gate-sequence identity.

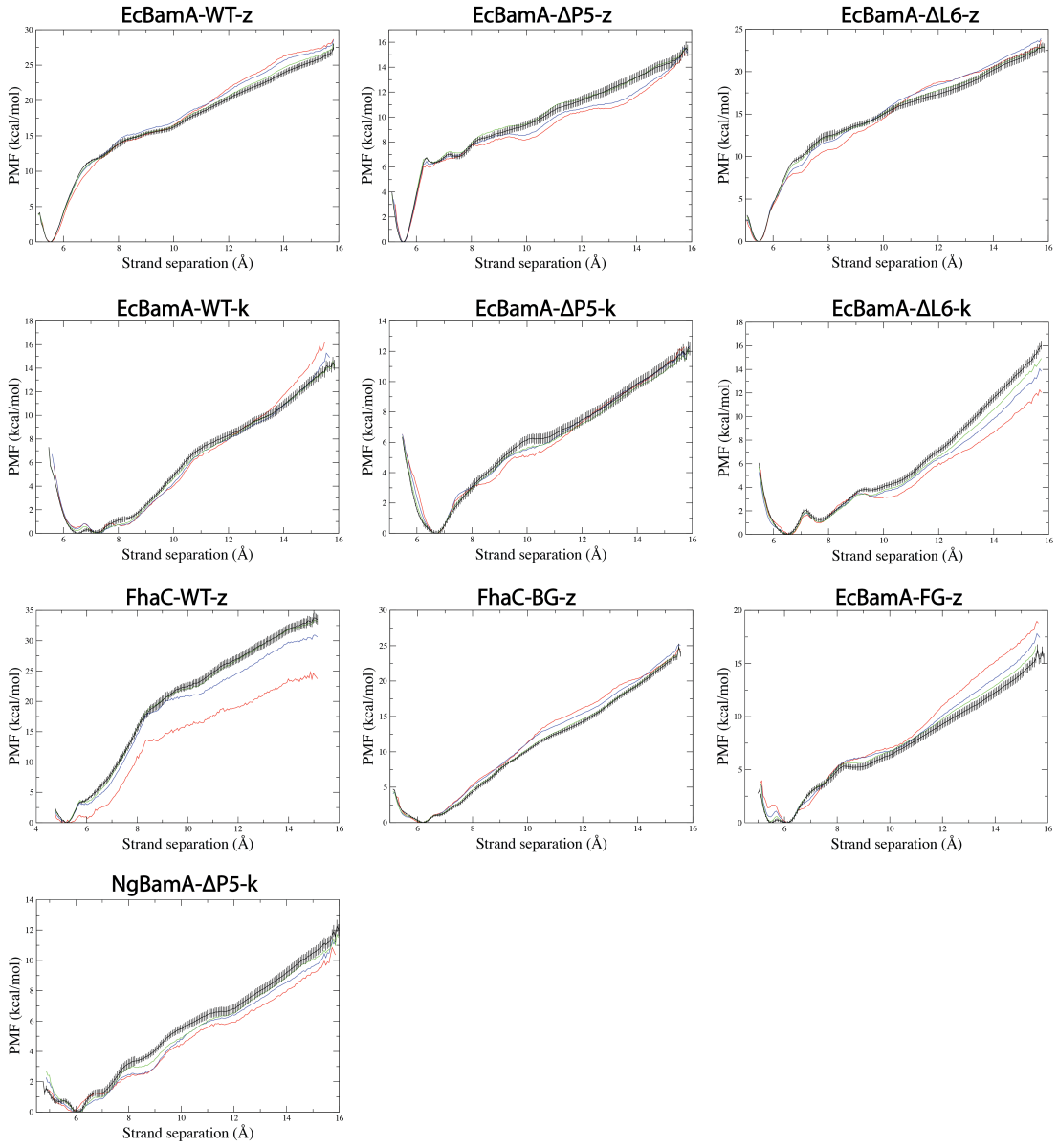

Figure B.5: Convergence of PMFs shown by plotting 2.5 ns (red), 5.0 ns (blue), 7.5 ns (green), and 20.0 ns (black) per replica for each of the PMFs determined for this study. Statistical error bars are shown for the 20.0 ns per replica trace.

systems to address the origin of the apparent lateral gate instability of BamA. In each of these systems, the two lateral gate strands from FhaC or BamA were replaced with those from the other. The first gate-replacement system, EcBamA with the FhaC gate (EcBamA-FG-z), consisted of EcBamA with the residues from strands β1 and β16 mutated to the corresponding residues of FhaC. The second system, FhaC with a BamA gate (FhaC-BG-z), consisted of FhaC with gate-strand residues mutated to the corresponding residues in EcBamA.

The resulting PMFs, shown in Fig. B.4, were surprising in the sense that the gate-replacement PMFs did not lie between the wild-type PMFs. The data indicate that in both gate-replacement systems, the gate interactions are disrupted by external factors preventing the gate strands' backbones from properly forming hydrogen bonds (Fig. B.6). Beyond a strand separation of about 8.5 Å, i.e., when contacts between gate strands are lost, FhaC-BG-z has a higher PMF value than BamA-FG-z, suggesting that the rest of the β-barrel dominates here. The particular gate residues, therefore, play little to no role in modulating the opening energy beyond the initial strand-separation phase.

L6 and P5 deletions decrease opening energy in zipped starting states. After investigating the role of the lateral-gate sequence on gate-opening energy, we sought to further determine energetic contributions external to the gate by modifying two other structurally significant moieties. The extracellular loop 6 (L6) contains a highly conserved four-residue motif (VRGF/Y), which interacts with conserved residues on β16 [21]. The fifth POTRA domain (P5) is one of up to five N-terminal periplasmic domains, which are thought to act as a scaffold onto which the other members of the BAM complex assemble, in addition to playing a role in initial substrate recognition and binding [20, 110, 88]. P5 is the only essential POTRA domain for BamA function [111], and it forms several interactions with periplasmic residues on the barrel domain.

To address the energetic roles that L6 and P5 may play in lateral gate opening, we determined PMFs of two systems, one with a deletion of L6 (EcBamA-ΔL6-z), and another

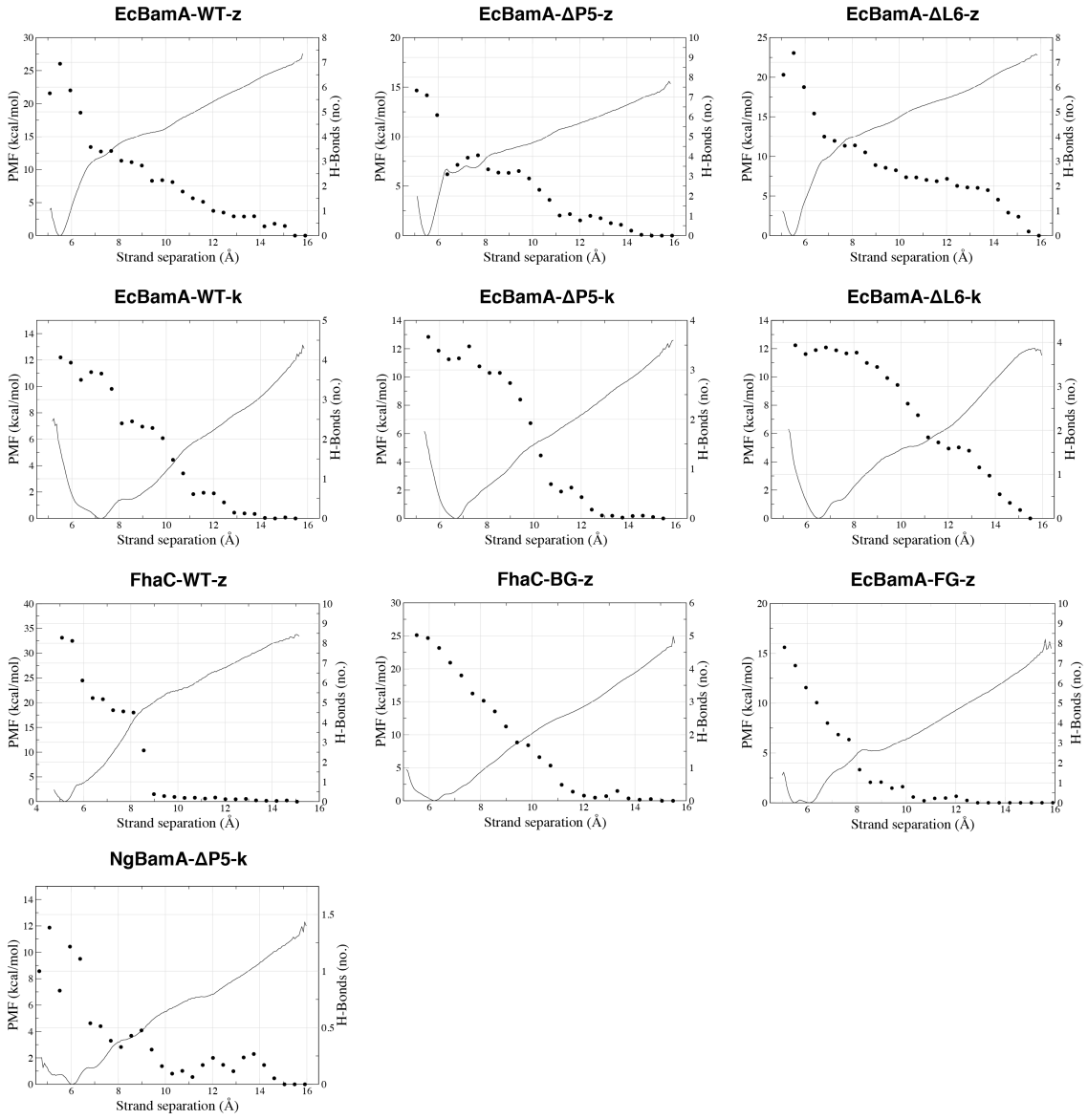

Figure B.6: Each PMF is shown alongside the number of lateral gate hydrogen bonds vs. strand separation. H-bonds are shown as black dots, PMFs are shown as black lines. These plots attempt to show the extent to which the PMF magnitude is derived from lateral gate hydrogen bonds.

with a deletion of P5 (EcBamA-ΔP5-z). The results of these simulations are shown in Fig. B.3 along with wild-type EcBamA for reference. EcBamA-ΔL6-z exhibits a modest decrease in opening energy with a PMF profile that follows that of EcBamA-WT-z rather closely. The only departure (2-3 kcal/mol) occurs between 6.5 and 7.5 Å of separation and could be due hydrogen bonds between L1 and L6 that are broken in this region for EcBamA-WT-z (Fig. B.7). EcBamA-ΔP5-z follows the wild type PMF remarkably well for values near the minimum before undergoing a sharp transition at a strand separation around 6.5 Å, beyond which the PMF follows a nearly linear increase with a smaller slope than that of EcBamA-WT-z.

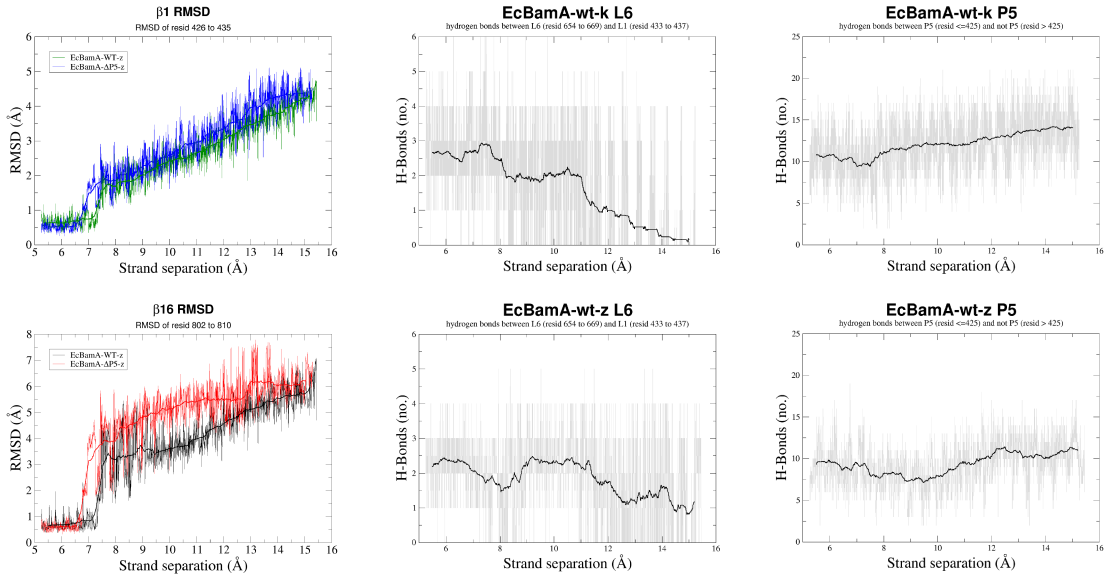

Figure B.7: RMSD and H-bonds plots for L6 and P5 over the course of REMD simulations. Decrease in the number of H-bonds in L6 with increasing strand separation may be responsible for decrease seen in EcBamA-ΔL6-z PMF. While there is no clear trend for the number of P5 H-bonds vs. strand separation, the sharp increase in β16 RMSD in EcBamA-ΔP5-z over EcBamA-WT-z, may be responsible for sharp shift seen in EcBamA-ΔP5-z PMF.

L6 and P5 deletions increase opening energy in kinked starting states. In contrast to the zipped states, the lateral gate opening energy for the deletion mutants is larger than that of EcBamA-WT when all are in the kinked state. Thus, with both L6 and P5 present,

the BamA gate is actually slightly less stable than without one of them, suggesting that they favor gate opening. An important role for both P5 and L6 is supported by experiments that have shown each is necessary for bacterial survival. In *E. coli*, deletion of P5 is lethal [88], while deletion of L6 causes significant impairment [20]. Additionally, mutation of the highly conserved VRGF/Y motif in L6 was shown to be lethal in two separate studies [112, 20].

Analysis of barrel stiffness reveals three main categories. Most of the PMFs shown thus far have significant qualitative differences between the early opening phase and the late opening phase. The late opening phase, i.e., beyond a strand separation of about 10 Å, is linear, whereas the early opening phase is often more erratic and dependent on the particular composition and conformation of the gate strands. We can isolate the factors modulating the barrel flexibility alone by plotting the average value of the slopes of the PMFs in the late phase, i.e., between 10 Å and 15 Å, together. These slopes, which represent an effective resistance to opening, fall into three main groups (Fig. B.8).

The first group consists of NgBamA-ΔP5-k, EcBamA-ΔP5-z, and EcBamA-ΔP5-k, all of which are missing the P5 domain. The second group with intermediate slopes is occupied by EcBamA-WT-z and modified systems based on EcBamA, namely EcBamA-FG-z, EcBamA-ΔL6-z, EcBamA-WT-k, and EcBamA-ΔL6-k. The third group, that with the highest slopes, is occupied by FhaC-WT-z and the FhaC-BG-z hybrid structure. In all of these groups, one can see that modification of gate residues or deletion of L6 has little effect on the energetic profile beyond initial separation. In contrast, P5 deletion has a significant effect on the energetics of opening. L6 is thought to play a significant structural role in BamA with interacting motifs on L6 and β16 that are both highly conserved [20], whereas P5 is thought to play a significant role in substrate recognition [110, 88].

Calculating the average slope of lateral-gate-separation energy revealed three main groups with distinct opening resistance. Barrel identity (FhaC or BamA) as well as presence or absence of the P5 moiety are clear contributors to the energy, whereas it is invariant

to the presence of L6 or lateral gate sequence. This is consistent with the idea that the lateral gate strands interact minimally above certain levels of strand separation. However, since P5 interacts with many periplasmic loop residues over a wide range of strand separation values, it is not surprising that this domain has a large effect on the energetic profile.

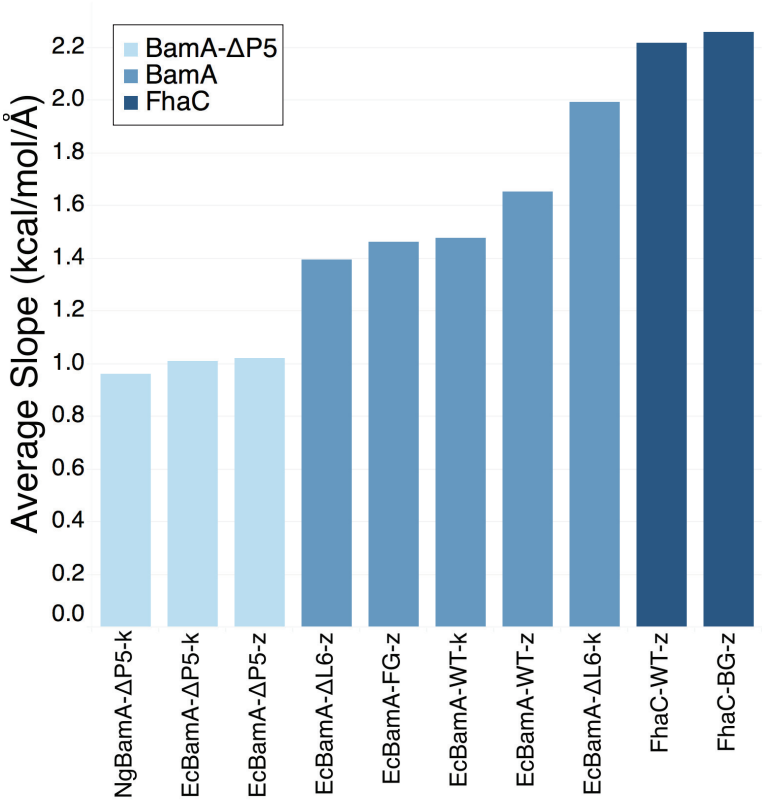

Figure B.8: Average slope of each PMF from 10 Å to 15 Å reveals three main categories of β-barrel stiffness. Those with a FhaC barrel demonstrate the highest resistance to barrel opening, EcBamA with P5 the next highest, and finally BamA without P5 the lowest.

REFERENCES

[1] W. B. Whitman, D. C. Coleman, and W. J. Wiebe, "Prokaryotes: The unseen majority," *Proc. Natl. Acad. Sci. USA*, vol. 95, pp. 6578–6583, 1998.

[2] R. Sender, S. Fuchs, and R. Milo, "Are We Really Vastly Outnumbered? Revisiting the Ratio of Bacterial to Host Cells in Humans," *Cell*, vol. 164, no. 3, pp. 337–340, 2016.

[3] S. P. Brown, D. M. Cornforth, and N. Mideo, "Evolution of virulence in opportunistic pathogens: generalism, plasticity, and control," *Trends Microbiol.*, vol. 20, no. 7, pp. 336–342, 2012.

[4] U.S. Department of Health and Human Services, Centers for Disease Control and Prevention, *Antibiotic resistance threats in the United States*, 2013.

[5] K. M. Storek, M. R. Auerbach, H. Shi, N. K. Garcia, D. Sun, N. N. Nickerson, R. Vij, Z. Lin, N. Chiang, K. Schneider, A. T. Wecksler, E. Skippington, G. Nakamura, D. Seshasayee, J. T. Koerber, J. Payandeh, P. A. Smith, and S. T. Rutherford, "Monoclonal antibody targeting the β-barrel assembly machine of Escherichia coli is bactericidal," *Proc. Natl. Acad. Sci. U.S.A.*, vol. 115, no. 14, pp. 3692–3697, Apr. 2018.

[6] R. Vij, Z. Lin, N. Chiang, J. M. Vernes, K. M. Storek, S. Park, J. Chan, Y. G. Meng, L. Comps-Agrar, P. Luan, S. Lee, K. Schneider, J. Bevers, I. Zilberleyb, C. Tam, C. M. Koth, M. Xu, A. Gill, M. R. Auerbach, P. A. Smith, S. T. Rutherford, G. Nakamura, D. Seshasayee, J. Payandeh, and J. T. Koerber, "A targeted boost-and-sort immunization strategy using Escherichia coli BamA identifies rare growth inhibitory antibodies," *Sci Rep*, vol. 8, no. 1, p. 7136, 2018.

[7] G. Andolina, L. C. Bencze, K. Zerbe, M. Müller, J. Steinmann, H. Kocherla, M. Mondal, J. Sobek, K. Moehle, G. Malojčić, B. Wollscheid, and J. A. Robinson, "A Peptidomimetic Antibiotic Interacts with the Periplasmic Domain of LptD from Pseudomonas aeruginosa," *ACS Chem. Biol.*, vol. 13, no. 3, pp. 666–675, 2018.

[8] S. U. Vetterli, K. Moehle, and J. A. Robinson, "Synthesis and antimicrobial activity against Pseudomonas aeruginosa of macrocyclic β-hairpin peptidomimetic antibiotics containing N-methylated amino acids," *Bioorg. Med. Chem.*, vol. 24, no. 24, pp. 6332–6339, Dec. 2016.

[9] K. Zerbe, K. Moehle, and J. A. Robinson, "Protein Epitope Mimetics: From New Antibiotics to Supramolecular Synthetic Vaccines," *Acc. Chem. Res.*, vol. 50, no. 6, pp. 1323–1331, Jun. 2017.

[10] H. C. Gram, "Über die isolierte färbung der schizomyceten in schnitt- und trockenpräparaten," *Fortschritte der Medizin*, vol. 2, pp. 185–89, 1884.

[11] R. AUSTRIAN, "The Gram stain and the etiology of lobar pneumonia, an historical note," *Bacteriol Rev*, vol. 24, no. 3, pp. 261–265, 1960.

[12] H. Nikaido and M. Vaara, "Molecular basis of bacterial outer membrane permeability," *Microbiol. Rev.*, vol. 49, pp. 1–32, 1985.

[13] H. Nikaido, "Molecular basis of bacterial outer membrane permeability revisited," *Microbiol. Mol. Biol. Rev.*, vol. 67, pp. 593–656, 2003.

[14] C. L. Hagan, T. J. Silhavy, and D. Kahne, "β-Barrel membrane protein assembly by the Bam complex," *Annu. Rev. Biochem.*, vol. 80, pp. 189–210, 2011.

[15] K. H. Kim, S. Aulakh, and M. Paetzel, "The bacterial outer membrane β-barrel assembly machinery," *Protein Sci.*, vol. 21, pp. 751–768, 2012.

[16] R. Voulhoux, M. P. Bos, J. Geurtsen, M. Mols, and J. Tommassen, "Role of a highly conserved bacterial protein in outer membrane protein assembly," *Science*, vol. 299, pp. 262–265, 2003.

[17] J. Bakelar, S. K. Buchanan, and N. Noinaj, "The structure of the β-barrel assembly machinery complex," *Science*, vol. 351, pp. 180–186, 2016.

[18] L. Han, J. Zheng, Y. Wang, X. Yang, Y. Liu, C. Sun, B. Cao, H. Zhou, D. Ni, J. Lou, Y. Zhao, and Y. Huang, "Structure of the BAM complex and its implications for biogenesis of outer-membrane proteins," *Nat. Struct. Mol. Biol.*, vol. 23, pp. 192–196, 2016.

[19] Y. Gu, H. Li, H. Dong, Y. Zeng, Z. Zhang, N. G. Paterson, P. J. Stansfeld, Z. Wang, Y. Zhang, W. Wang, and C. Dong, "Structural basis of outer membrane protein insertion by the BAM complex," *Nature*, vol. 531, pp. 64–69, 2016.

[20] N. Noinaj, A. J. Kuszak, J. C. Gumbart, P. Lukacik, H. Chang, N. C. Easley, T. Lithgow, and S. K. Buchanan, "Structural insight into the biogenesis of β-barrel membrane proteins," *Nature*, vol. 501, pp. 385–390, 2013.

[21] N. Noinaj, A. J. Kuszak, C. Balusek, J. C. Gumbart, and S. K. Buchanan, "Lateral opening and exit pore formation are required for BamA function," *Structure*, vol. 22, pp. 1055–1062, 2014.

[22] J. H. Kleinschmidt, T. den Blaauwen, A. J. Driessen, and L. K. Tamm, "Outer membrane protein A of Escherichia coli inserts and folds into lipid bilayers by a concerted mechanism," *Biochemistry*, vol. 38, no. 16, pp. 5006–5016, 1999.

[23] G. H. Huysmans, S. E. Radford, D. J. Brockwell, and S. A. Baldwin, "The N-terminal helix is a post-assembly clamp in the bacterial outer membrane protein PagP," *J. Mol. Biol.*, vol. 373, no. 3, pp. 529–540, 2007.

[24] N. K. Burgess, T. P. Dao, A. M. Stanley, and K. G. Fleming, "Beta-barrel proteins that reside in the Escherichia coli outer membrane in vivo demonstrate varied folding behavior in vitro," *J. Biol. Chem.*, vol. 283, pp. 26 748–26 758, 2008.

[25] A. M. Stanley and K. G. Fleming, "The process of folding proteins into membranes: challenges and progress," *Arch. Biochem. Biophys.*, vol. 469, no. 1, pp. 46–66, 2008.

[26] C. P. Moon and K. G. Fleming, "Side-chain hydrophobicity scale derived from transmembrane protein folding into lipid bilayers," *Proc. Natl. Acad. Sci. USA*, vol. 108, pp. 10 174–10 177, 2011.

[27] D. Gessmann, Y. H. Chung, E. J. Danoff, A. M. Plummer, C. W. Sandlin, N. R. Zaccai, and K. G. Fleming, "Outer membrane β-barrel protein folding is physically controlled by periplasmic lipid head groups and BamA," *Proc. Natl. Acad. Sci. U.S.A.*, vol. 111, pp. 5878–5883, 2014.

[28] E. J. Danoff and K. G. Fleming, "Membrane defects accelerate outer membrane β-barrel protein folding," *Biochemistry*, vol. 54, pp. 97–99, 2015.

[29] P. A. Doerner and M. C. Sousa, "Extreme Dynamics in the BamA β-Barrel Seam," *Biochemistry*, vol. 56, pp. 3142–3149, 2017.

[30] I. E. Gentle, L. Burri, and T. Lithgow, "Molecular architecture and function of the Omp85 family of proteins," *Mol. Microbiol.*, vol. 58, no. 5, pp. 1216–1225, 2005.

[31] B. van den Berg, "Lateral gates: β-barrels get in on the act," *Nat. Struct. Mol. Biol.*, vol. 20, pp. 1237–1239, 2013.

[32] A. I. C. Hohr, C. Lindau, C. Wirth, J. Qiu, D. A. Stroud, S. Kutik, B. Guiard, C. Hunte, T. Becker, N. Pfanner, and N. Wiedemann, "Membrane protein insertion through a mitochondrial β-barrel gate," *Science*, vol. 359, no. 6373, Jan. 2018.

[33] C. Whitfield and M. S. Trent, "Biosynthesis and export of bacterial lipopolysaccharides," *Annu. Rev. Biochem.*, vol. 83, pp. 99–128, 2014.

[34] N. Ruiz, D. Kahne, and T. J. Silhavy, "Transport of lipopolysaccharide across the cell envelope: the long road of discovery," *Nat. Rev. Microbiol.*, vol. 7, no. 9, pp. 677–683, 2009.

[35] G. Zhang, T. C. Meredith, and D. Kahne, "On the essentiality of lipopolysaccharide to Gram-negative bacteria," *Curr. Opin. Microbiol.*, vol. 16, no. 6, pp. 779–785, 2013.

[36] R. Villa, A. M. Martorana, S. Okuda, L. J. Gourlay, M. Nardini, P. Sperandeo, G. Dehò, M. Bolognesi, D. Kahne, and A. Polissi, "The Escherichia coli Lpt transenvelope protein complex for lipopolysaccharide export is assembled via conserved structurally homologous domains," *J. Bacteriol.*, vol. 195, no. 5, pp. 1100–1108, 2013.

[37] S. S. Chng, L. S. Gronenberg, and D. Kahne, "Proteins required for lipopolysaccharide assembly in Escherichia coli form a transenvelope complex," *Biochemistry*, vol. 49, no. 22, pp. 4565–4567, 2010.

[38] S. Narita and H. Tokuda, "Biochemical characterization of an ABC transporter LptBFGC complex required for the outer membrane sorting of lipopolysaccharides," *FEBS Lett.*, vol. 583, no. 13, pp. 2160–2164, 2009.

[39] P. Sperandeo, R. Villa, A. M. Martorana, M. Samalikova, R. Grandori, G. Dehò, and A. Polissi, "New insights into the Lpt machinery for lipopolysaccharide transport to the cell surface: LptA-LptC interaction and LptA stability as sensors of a properly assembled transenvelope complex," *J. Bacteriol.*, vol. 193, no. 5, pp. 1042–1053, 2011.

[40] A. X. Tran, C. Dong, and C. Whitfield, "Structure and functional analysis of LptC, a conserved membrane protein involved in the lipopolysaccharide export pathway in Escherichia coli," *J. Biol. Chem.*, vol. 285, no. 43, pp. 33 529–33 539, 2010.

[41] S. Qiao, Q. Luo, Y. Zhao, X. C. Zhang, and Y. Huang, "Structural basis for lipopolysaccharide insertion in the bacterial outer membrane," *Nature*, vol. 511, no. 7507, pp. 108–111, 2014.

[42] D. J. Sherman, R. Xie, R. J. Taylor, A. H. George, S. Okuda, P. J. Foster, D. J. Needleman, and D. Kahne, "Lipopolysaccharide is transported to the cell surface by a membrane-to-membrane protein bridge," *Science*, vol. 359, no. 6377, pp. 798–801, Feb. 2018.

[43] H. Dong, Q. Xiang, Y. Gu, Z. Wang, N. G. Paterson, P. J. Stansfeld, C. He, Y. Zhang, W. Wang, and C. Dong, "Structural basis for outer membrane lipopolysaccharide insertion," *Nature*, vol. 511, no. 7507, pp. 52–56, 2014.

[44] R. E. Bishop, "Structural biology: Lipopolysaccharide rolls out the barrel," *Nature*, vol. 511, no. 7507, pp. 37–38, 2014.

[45] K. Lundquist, J. Bakelar, N. Noinaj, and J. C. Gumbart, "C-terminal kink formation is required for lateral gating in BamA," *Proc. Natl. Acad. Sci. U.S.A.*, vol. 115, no. 34, E7942–E7949, Aug. 2018.

[46] R. S. Bamert, K. Lundquist, H. Hwang, C. T. Webb, T. Shiota, C. J. Stubenrauch, M. J. Belousoff, R. J. A. Goode, R. B. Schittenhelm, R. Zimmerman, M. Jung, J. C. Gumbart, and T. Lithgow, "Structural basis for substrate selection by the translocation and assembly module of the β-barrel assembly machinery," *Mol. Microbiol.*, vol. 106, pp. 142–156, 2017.

[47] I. Botos, N. Majdalani, S. J. Mayclin, J. G. McCarthy, K. Lundquist, D. Wojtowicz, T. J. Barnard, J. C. Gumbart, and S. K. Buchanan, "Structural and Functional Characterization of the LPS Transporter LptDE from Gram-Negative Pathogens," *Structure*, vol. 24, no. 6, pp. 965–976, Jun. 2016.

[48] C. Dong, K. Beis, J. Nesper, A. L. Brunkan-Lamontagne, B. R. Clarke, C. Whitfield, and J. H. Naismith, "Wza the translocon for E. coli capsular polysaccharides defines a new class of membrane protein," *Nature*, vol. 444, pp. 226–229, 2006.

[49] J. S. Slusky, "Outer membrane protein design," *Curr. Opin. Struct. Biol.*, vol. 45, pp. 45–52, 2017.

[50] C. T. Webb, E. Heinz, and T. Lithgow, "Evolution of the β-barrel assembly machinery," *Trends Microbiol.*, vol. 20, pp. 612–620, 2012.

[51] R. Koebnik, K. P. Locher, and P. Van Gelder, "Structure and function of bacterial outer membrane proteins: barrels in a nutshell," *Mol. Microbiol.*, vol. 37, pp. 239–253, 2000.

[52] N. Noinaj, N. C. Easley, M. Oke, N. Mizuno, J. Gumbart, E. Boura, A. N. Steere, O. Zak, P. Aisen, E. Tajkhorshid, R. W. Evans, A. R. Gorringe, A. B. Mason, A. C. Steven, and S. K. Buchanan, "Structural basis for iron piracy by pathogenic Neisseria," *Nature*, vol. 483, pp. 53–58, 2012.

[53] J. H. Jiang, J. Tong, K. S. Tan, and K. Gabriel, "From evolution to pathogenesis: the link between β-barrel assembly machineries in the outer membrane of mitochondria and gram-negative bacteria," *Int. J. Mol. Sci.*, vol. 13, pp. 8038–8050, 2012.

[54] J. G. Sklar, T. Wu, D. Kahne, and T. J. Silhavy, "Defining the roles of the periplasmic chaperones SurA, Skp, and DegP in Escherichia coli," *Genes Dev.*, vol. 21, pp. 2473–2484, 2007.

[55] C. P. Moon, N. R. Zaccai, P. J. Fleming, D. Gessmann, and K. G. Fleming, "Membrane protein thermodynamic stability may serve as the energy sink for sorting in the periplasm," *Proc. Natl. Acad. Sci. U.S.A.*, vol. 110, pp. 4285–4290, 2013.

[56] S. M. Costello, A. M. Plummer, P. J. Fleming, and K. G. Fleming, "Dynamic periplasmic chaperone reservoir facilitates biogenesis of outer membrane proteins," *Proc. Natl. Acad. Sci. U.S.A.*, vol. 113, E4794–4800, 2016.

[57] R. Sikdar, J. H. Peterson, D. E. Anderson, and H. D. Bernstein, "Folding of a bacterial integral outer membrane protein is initiated in the periplasm," *Nat. Commun.*, vol. 8, p. 1309, 2017.

[58] T. Wu, J. Malinverni, N. Ruiz, S. Kim, T. J. Silhavy, and D. Kahne, "Identification of a multicomponent complex required for outer membrane biogenesis in *Escherichia coli*," *Cell*, vol. 121, pp. 235–245, 2005.

[59] C. L. Hagan, S. Kim, and D. Kahne, "Reconstitution of outer membrane protein assembly from purified components," *Science*, vol. 328, pp. 890–892, 2010.

[60] M. P. Bos, V. Robert, and J. Tommassen, "Biogenesis of the gram-negative bacterial outer membrane," *Annu. Rev. Microbiol.*, vol. 61, pp. 191–214, 2007.

[61] D. P. Ricci and T. J. Silhavy, "The Bam machine: a molecular cooper," *Biochim. Biophys. Acta*, vol. 1818, pp. 1067–1084, 2012.

[62] T. J. Knowles, A. Scott-Tucker, M. Overduin, and I. R. Henderson, "Membrane protein architects: the role of the BAM complex in outer membrane protein assembly," *Nat. Rev. Microbiol.*, vol. 7, pp. 206–214, 2009.

[63] S. E. Rollauer, M. A. Sooreshjani, N. Noinaj, and S. K. Buchanan, "Outer membrane protein biogenesis in Gram-negative bacteria," *Philos. Trans. R. Soc. Lond., B, Biol. Sci.*, vol. 370, 2015.

[64] M. G. Iadanza, A. J. Higgins, B. Schiffrin, A. N. Calabrese, D. J. Brockwell, A. E. Ashcroft, S. E. Radford, and N. A. Ranson, "Lateral opening in the intact β-barrel assembly machinery captured by cryo-EM," *Nat. Commun.*, vol. 7, p. 12 865, 2016.

[65] E. Heinz and T. Lithgow, "A comprehensive analysis of the Omp85/TpsB protein superfamily structural diversity, taxonomic occurrence, and evolution," *Front Microbiol*, vol. 5, p. 370, 2014.

[66] E. Heinz, J. Selkrig, M. J. Belousoff, and T. Lithgow, "Evolution of the Translocation and Assembly Module (TAM)," *Genome Biol Evol*, vol. 7, no. 6, pp. 1628–1643, 2015.

[67] D. Marsh, B. Shanmugavadivu, and J. H. Kleinschmidt, "Membrane elastic fluctuations and the insertion and tilt of beta-barrel proteins," *Biophys. J.*, vol. 91, pp. 227–232, 2006.

[68] C. L. Pocanschi, G. J. Patel, D. Marsh, and J. H. Kleinschmidt, "Curvature elasticity and refolding of OmpA in large unilamellar vesicles," *Biophys. J.*, vol. 91, pp. L75–77, 2006.

[69] D. Ni, Y. Wang, X. Yang, H. Zhou, X. Hou, B. Cao, Z. Lu, X. Zhao, K. Yang, and Y. Huang, "Structural and functional analysis of the β-barrel domain of BamA from Escherichia coli," *FASEB J.*, vol. 28, pp. 2677–2685, 2014.

[70] R. Albrecht, M. Schutz, P. Oberhettinger, M. Faulstich, I. Bermejo, T. Rudel, K. Diederichs, and K. Zeth, "Structure of BamA, an essential factor in outer membrane protein biogenesis," *Acta Crystallogr. D Biol. Crystallogr.*, vol. 70, pp. 1779–1789, 2014.

[71] J. H. Kleinschmidt and L. K. Tamm, "Secondary and tertiary structure formation of the beta-barrel membrane protein OmpA is synchronized and depends on membrane thickness," *J. Mol. Biol.*, vol. 324, pp. 319–330, 2002.

[72] C. Balusek and J. C. Gumbart, "Role of the Native Outer-Membrane Environment on the Transporter BtuB," *Biophys. J.*, vol. 111, pp. 1409–1417, 2016.

[73] A. Pavlova, H. Hwang, K. Lundquist, C. Balusek, and J. C. Gumbart, "Living on the edge: Simulations of bacterial outer-membrane proteins," *Biochim. Biophys. Acta*, vol. 1858, pp. 1753–1759, 2016.

[74] T. Maier, B. Clantin, F. Gruss, F. Dewitte, A. S. Delattre, F. Jacob-Dubuisson, S. Hiller, and V. Villeret, "Conserved Omp85 lid-lock structure and substrate recognition in FhaC," *Nat. Commun.*, vol. 6, p. 7452, 2015.

[75] S. Y. Sheu, D. Y. Yang, H. L. Selzle, and E. W. Schlag, "Energetics of hydrogen bonds in peptides," *Proc. Natl. Acad. Sci. U.S.A.*, vol. 100, pp. 12 683–12 687, 2003.

[76] A. Szabo, K. Schulten, and Z. Schulten, "First passage time approach to diffusion controlled reactions," *J. Chem. Phys.*, vol. 72, pp. 4350–4357, 1980.

[77] J. H. Kleinschmidt, P. V. Bulieris, J. Qu, M. Dogterom, and T. den Blaauwen, "Association of neighboring β-strands of outer membrane protein A in lipid bilayers revealed by site-directed fluorescence quenching," *J. Mol. Biol.*, vol. 407, pp. 316–332, 2011.

[78] C. Stubenrauch, M. J. Belousoff, I. D. Hay, H. H. Shen, J. Lillington, K. L. Tuck, K. M. Peters, M. D. Phan, A. W. Lo, M. A. Schembri, R. A. Strugnell, G. Waksman,

and T. Lithgow, "Effective assembly of fimbriae in Escherichia coli depends on the translocation assembly module nanomachine," *Nat. Microbiol.*, vol. 1, p. 16 064, 2016.

[79] N. Paramasivam, M. Habeck, and D. Linke, "Is the C-terminal insertional signal in Gram-negative bacterial outer membrane proteins species-specific or not?" *BMC Genomics*, vol. 13, p. 510, 2012.

[80] K. Anwari, S. Poggio, A. Perry, X. Gatsos, S. H. Ramarathinam, N. A. Williamson, N. Noinaj, S. Buchanan, K. Gabriel, A. W. Purcell, C. Jacobs-Wagner, and T. Lithgow, "A modular BAM complex in the outer membrane of the alpha-proteobacterium Caulobacter crescentus," *PLoS ONE*, vol. 5, no. 1, e8619, 2010.

[81] R. Albrecht and K. Zeth, "Structural basis of outer membrane protein biogenesis in bacteria," *J. Biol. Chem.*, vol. 286, no. 31, pp. 27 792–27 803, 2011.

[82] K. H. Kim and M. Paetzel, "Crystal structure of Escherichia coli BamB, a lipoprotein component of the β-barrel assembly machinery complex," *J. Mol. Biol.*, vol. 406, no. 5, pp. 667–678, 2011.

[83] N. Noinaj, J. W. Fairman, and S. K. Buchanan, "The crystal structure of BamB suggests interactions with BamA and its role within the BAM complex," *J. Mol. Biol.*, vol. 407, no. 2, pp. 248–260, 2011.

[84] K. H. Kim, S. Aulakh, W. Tan, and M. Paetzel, "Crystallographic analysis of the C-terminal domain of the Escherichia coli lipoprotein BamC," *Acta Crystallogr. Sect. F Struct. Biol. Cryst. Commun.*, vol. 67, no. Pt 11, pp. 1350–1358, 2011.

[85] L. R. Warner, K. Varga, O. F. Lange, S. L. Baker, D. Baker, M. C. Sousa, and A. Pardi, "Structure of the BamC two-domain protein obtained by Rosetta with a limited NMR data set," *J. Mol. Biol.*, vol. 411, no. 1, pp. 83–95, 2011.

[86] C. M. Sandoval, S. L. Baker, K. Jansen, S. I. Metzner, and M. C. Sousa, "Crystal structure of BamD: an essential component of the β-Barrel assembly machinery of gram-negative bacteria," *J. Mol. Biol.*, vol. 409, no. 3, pp. 348–357, 2011.

[87] C. Dong, H. F. Hou, X. Yang, Y. Q. Shen, and Y. H. Dong, "Structure of Escherichia coli BamD and its functional implications in outer membrane protein assembly," *Acta Crystallogr. D Biol. Crystallogr.*, vol. 68, no. Pt 2, pp. 95–101, 2012.

[88] S. Kim, J. C. Malinverni, P. Sliz, T. J. Silhavy, S. C. Harrison, and D. Kahne, "Structure and function of an essential component of the outer membrane protein assembly machine," *Science*, vol. 317, pp. 961–964, 2007.

[89] N. Noinaj, S. E. Rollauer, and S. K. Buchanan, "The β-barrel membrane protein insertase machinery from Gram-negative bacteria," *Curr. Opin. Struct. Biol.*, vol. 31, pp. 35–42, 2015.

[90] P. K. O'Neil, S. E. Rollauer, N. Noinaj, and S. K. Buchanan, "Fitting the Pieces of the β-Barrel Assembly Machinery Complex," *Biochemistry*, vol. 54, no. 41, pp. 6303–6311, 2015.

[91] P. J. Fleming, D. S. Patel, E. L. Wu, Y. Qi, M. S. Yeom, M. C. Sousa, K. G. Fleming, and W. Im, "BamA POTRA Domain Interacts with a Native Lipid Membrane Surface," *Biophys. J.*, vol. 110, pp. 2698–2709, 2016.

[92] L. Maragliano, A. Fischer, E. Vanden-Eijnden, and G. Ciccotti, "String method in collective variables: Minimum free energy paths and isocommittor surfaces," *J. Chem. Phys.*, vol. 125, p. 24 106, 2006.

[93] B. Schiffrin, D. J. Brockwell, and S. E. Radford, "Outer membrane protein folding from an energy landscape perspective," *BMC Biol.*, vol. 15, no. 1, p. 123, Dec. 2017.

[94] N. Ruiz, D. Kahne, and T. J. Silhavy, "Advances in understanding bacterial outer-membrane biogenesis," *Nat. Rev. Microbiol.*, vol. 4, no. 1, pp. 57–66, 2006.

[95] Y. Gu, P. J. Stansfeld, Y. Zeng, H. Dong, W. Wang, and C. Dong, "Lipopolysaccharide is inserted into the outer membrane through an intramembrane hole, a lumen gate, and the lateral opening of LptD," *Structure*, vol. 23, no. 3, pp. 496–504, 2015.

[96] J. C. Phillips, R. Braun, W. Wang, J. Gumbart, E. Tajkhorshid, E. Villa, C. Chipot, R. D. Skeel, L. Kale, and K. Schulten, "Scalable molecular dynamics with NAMD," *J. Comput. Chem.*, vol. 26, pp. 1781–1802, 2005.

[97] J. B. Klauda, R. M. Venable, J. A. Freites, J. W. O'Connor, D. J. Tobias, C. Mondragon-Ramirez, I. Vorobyov, A. D. MacKerell Jr., and R. W. Pastor, "Update of the CHARMM all-atom additive force field for lipids: Validation on six lipid types," *J. Phys. Chem. B*, vol. 114, pp. 7830–7843, 2010.

[98] T. A. Darden, D. M. York, and L. G. Pedersen, "Particle mesh Ewald: An N log N method for Ewald sums in large systems," *J. Chem. Phys.*, vol. 98, pp. 10 089–10 092, 1993.

[99] J. C. Gumbart, I. Teo, B. Roux, and K. Schulten, "Reconciling the roles of kinetic and thermodynamic factors in membrane-protein insertion," *J. Am. Chem. Soc.*, vol. 135, pp. 2291–2297, 2013.

[100] Y. Sugita, A. Kitao, and Y. Okamoto, "Multidimensional Replica-Exchange Method for Free-Energy Calculations," *J. Chem. Phys.*, vol. 113, pp. 6042–6051, 2000.

[101] G. M. Torrie and J. P. Valleau, "Nonphysical sampling distributions in monte carlo free-energy estimation: Umbrella sampling," *J. Comput. Phys.*, vol. 23, pp. 187–199, 1997.

[102] S. Kumar, J. M. Rosenberg, D. Bouzida, R. H. Swendsen, and P. A. Kollman, "The weighted histogram analysis method for free-energy calculation on biomolecules.," *J. Comput. Chem.*, vol. 13, pp. 1011–1021, 1992.

[103] B. Roux, "The calculation of the potential of mean force using computer simulations," *Comput. Phys. Commun.*, vol. 91, pp. 275–282, 1995.

[104] E. Darve and A. Pohorille, "Calculating free energies using average force," *J. Chem. Phys.*, vol. 115, pp. 9169–9183, 2001.

[105] J. Gumbart, C. Chipot, and K. Schulten, "Free-energy cost for translocon-assisted insertion of membrane proteins," *Proc. Natl. Acad. Sci. USA*, vol. 108, pp. 3596–3601, 2011.

[106] J. Hénin and C. Chipot, "Overcoming free energy barriers using unconstrained molecular dynamics simulations," *J. Chem. Phys.*, vol. 121, no. 7, pp. 2904–2914, 2004.

[107] J. Schlitter, M. Engels, and P. Kruger, "Targeted molecular dynamics: A new approach for searching pathways of conformational transitions," *J. Mol. Graphics*, vol. 12, pp. 84–94, 1994.

[108] K. Gaalswyk, E. Awoonor-Williams, and C. N. Rowley, "Generalized Langevin Methods for Calculating Transmembrane Diffusivity," *J. Chem. Theory Comput.*, vol. 12, pp. 5609–5619, 2016.

[109] M. H. Olsson, C. R. Søndergaard, M. Rostkowski, and J. H. Jensen, "PROPKA3: Consistent Treatment of Internal and Surface Residues in Empirical pKa Predictions," *J. Chem. Theory Comput.*, vol. 7, pp. 525–537, 2011.

[110] P. Z. Gatzeva-Topalova, T. A. Walton, and M. C. Sousa, "Crystal structure of YaeT: conformational flexibility and substrate recognition," *Structure*, vol. 16, pp. 1873–1881, 2008.

[111] M. P. Bos, V. Robert, and J. Tommassen, "Functioning of outer membrane protein assembly factor Omp85 requires a single POTRA domain," *EMBO Rep.*, vol. 8, pp. 1149–1154, 2007.

[112] M. Leonard-Rivera and R. Misra, "Conserved residues of the putative L6 loop of Escherichia coli BamA play a critical role in the assembly of β-barrel outer membrane proteins, including that of BamA itself," *J. Bacteriol.*, vol. 194, pp. 4662–4668, 2012.

VITA

Karl Lundquist was born in 1988, in Pontiac Michigan. He grew up in Coldwater and Mount Pleasant, Michigan and attended High School at Mount Pleasant high school.

He attended The University of Michigan from 2007 to 2012 and graduated with a B.S. in Physics with a minor in Mathematics. While at Michigan he performed research in Atomic Physics with Professor Georg Raithel, aiding in the construction of a ^{87}Rb Rydberg atom guide and a Bose-Einstein condensate atom laser. This work culminated in two publications characterizing the dynamics of guided ^{87}Rb Rydberg atoms.

In 2012, he entered the Ph.D. program at the Georgia Institute of Technology, and in 2014 received a M.S. in Physics. At Georgia Tech, he developed an interest in biophysics through his work with optical tweezers on the rheology of the pericellular coats of mammalian cells with Professor Jennifer Curtis. He then pursued computational biophysics research under the guidance of Professor James Gumbart. Under Professor Gumbart, he studied the insertion mechanisms two outer membrane protein systems in Gram-negative bacteria using molecular dynamics. This work culminated in the authorship of five publications. Through this work he also developed a computational protocol to compute free-energies of conformational changes and their associated timescales.

Journal Articles

9. K. Lundquist and J.C. Gumbart, "The presence of lipopolysaccharide induces gate opening in LptD," *Biochim. Biophys. Acta Biomembr.*, Invited for publication Feb. 2019.

8. I. Fernandez, R. Baxter, J. Garcia Perez, D. Kong, E. Vendrame, T. Ranganath, K. Lundquist, T. Nguyen, J. Black, C. Galambos, J.C. Gumbart, N. Dawany, J. Kelsen, E. de Zoeten, K. Sullivan, C. Blish, R. Kedl, C. Dutmer, and E. Hsieh, "A Novel Human IL2RB Mutation Results in T and NK cell-driven Immune Dysregulation," *J. Exp. Med.*, Submitted Nov. 2018.

7. K. Lundquist, J. Bakelar, N. Noinaj, and J. C. Gumbart, "C-terminal kink formation

is required for lateral gating in BamA," *Proc. Natl. Acad. Sci. U.S.A.*, vol. 115, no. 34, E7942-E7949, Aug. 2018.

6. R. S. Bamert, K. Lundquist, H. Hwang, C. T. Webb, T. Shiota, C. J. Stubenrauch, M. J. Belousoff, R. J. A. Goode, R. B. Schittenhelm, R. Zimmerman, M. Jung, J. C. Gumbart, and T. Lithgow, "Structural basis for substrate selection by the translocation and assembly module of the β-barrel assembly machinery," *Mol. Microbiol.*, vol. 106, pp. 142156, 2017.

5. I. Botos, N. Majdalani, S. J. Mayclin, J. G. McCarthy, K. Lundquist, D. Wojtowicz, T. J. Barnard, J. C. Gumbart, and S. K. Buchanan, "Structural and Functional Characterization of the LPS Transporter LptDE from Gram-Negative Pathogens," *Structure*, vol. 24, no. 6, pp. 965976, Jun. 2016.

4. K. Lundquist, C. Herndon, T. H. Harty, and J.C. Gumbart, "Accelerating the use of molecular modeling in the high school classroom with VMD Lite," *Biochem. Mol. Biol. Educ.*, 44: pp. 124-129, 2016.

3. A. Pavlova, H. Hwang, K. Lundquist, C. Balusek, J. C. Gumbart, "Living on the edge: Simulations of bacterial outer-membrane proteins," *Biochim. Biophys. Acta Biomembr.*, vol. 1858, no. 7, pp. 1753-1759, 2016.

2. M. Traxler, R.E. Sapiro, K. Lundquist, E.P. Power, G. Raithel, "Coupled internal-state and center-of-mass dynamics of Rydberg atoms in a magnetic guide," *Phys. Rev. A*, vol. 87, no. 5, pp. 053418, 2013.

1. M. Traxler, R. E. Sapiro, C. Hempel, K. Lundquist, E. P. Power, and G. Raithel "Guiding of Rydberg atoms in a high-gradient magnetic guide," *Phys. Rev. A* vol. 86, no. 2, pp. 023414, 2012.

Book Chapters

1. C Balusek, H Hwang, A Hazel, K Lundquist, A Pavlova, "Diverse Protein-Folding Pathways and Functions of β-Hairpins and β-Sheets," Quantitative Models for Microscopic to Macroscopic Biological Macromolecules and Tissues. *Springer*, 2018